



Evaluation of Accelerometers for Pyroshock Performance in a Harsh Field Environment

Written By

Anthony Agnello & Robert Sill PCB Piezotronics, Inc., Depew, NY, USA
Patrick Walter Texas Christian University/PCB Consultant, Fort Worth, TX, USA
Strether Smith Independent Consultant, Cupertino, CA, USA

An evaluation of the performance of eight (8) different models of accelerometers in severe pyroshock environments has been planned, executed, and analyzed. These experiments showed that modern versions of accelerometers using both Mechanically Isolated Electrically Filtered Piezoelectric (MIEF-IEPE) and Micro Electromechanical Systems (MEMS) technology provided excellent results for excitations encountered in high-level pyrotechnic testing.

**Agnello, Anthony; Sill, Robert; Smith, Strether;
and Walter, Patrick**

Evaluation of Accelerometers for Pyroshock Performance in a Harsh Field Environment

Anthony Agnello and Robert Sill
PCB Piezotronics, Inc.
Depew, NY 14043

Patrick Walter
Texas Christian University/PCB Consultant
Fort Worth, TX 76129

Strether Smith
Independent Consultant
Cupertino, CA 95014

A series of experiments has been performed to evaluate the performance of eleven accelerometers commonly used in high level pyrotechnic shock tests. They included both mechanically isolated and electronically filtered piezoelectric and silicon (MEMS) based devices manufactured by Endevco and PCB Piezotronics. All had a range of 50KG or higher.

Five tests at different levels (quantity of explosive) emulated some of the more severe amplitude and frequency excitation that might be expected in laboratory-or field-based experiments. The higher level tests produced significant plastic deformation in the fixture. Accelerations on the order of 15 KG peak to 10,000 Hz were measured with indicated frequency content extending past 30 KHz.

The majority of the modern accelerometers performed far better than the authors expected. All exhibited some zero shift, which averaged between 0.02% and 0.25% of the peak-peak shock level accelerometer for the five tests. One outlier had an average offset of 0.94%. However, even these small errors severely compromised the SRS calculations at lower frequencies.

The technique used to reduce the effect of these offset errors is also presented to validate test results.

INTRODUCTION

If data quality is poor when measuring mechanical shock, it is common to blame the accelerometer. However, there are other contributors to this lack of success that need to be considered. These include: poor mounting surface for the accelerometer, improper accelerometer coupling (surface finish, torque, grease), large transverse acceleration inputs, cable issues (cable tie down, shielding, bend radii, stiffness, connector pin chatter, etc.), improper signal conditioning and data acquisition (over ranging, slew rate limiting, signal/noise, improper grounding, wrong input/output characteristics, ...), extraneous environmental inputs coupling into the measurement system, and many more. In addition, at times the environment that is attempted to be measured may be just too harsh for the accelerometer to operate in reliably.

During development testing of high-G accelerometers the main evaluation tool used by the accelerometer manufacturer is the Hopkinson Bar¹. Testing performed on this bar can achieve levels of over 100 KG and frequencies above 10 KHz, however, by design the motion it produces is essentially 1-dimensional. Comparative testing of a group of severe shock (high-G) accelerometers, primarily using a Hopkinson Bar, has been reported previously².

This work documents field testing performed at National Test Systems (NTS), Santa Clarita, CA. The test environment provided, described in detail below, was a series of explosive pyrotechnic events.

Two accelerometers types were tested:

1. Mechanically Isolated and Electrical Filtered Piezoelectric technology (denoted MIEF- IEPE) and
2. Micro ElectroMechanical Systems technology (denoted MEMS).

The MIEF- IEPE accelerometers had an internal elastomeric matrix to isolate the piezoelectric element from the high stresses encountered at their resonance excitation. An internal electrical filter reduced the effects of this isolation on frequency response up to and including 10 KHz.

The MEMS accelerometers had sculptured silicon dice manufactured with precision tolerances to effect over range stops and provide a small amount of damping (0.02 to 0.04 typical). They had nominal resonances of approximately 150 KHz. The one exception was the Model 7270, which had a damping ratio well below 0.01 and no mechanical stops. This was a byproduct of its resonance being approximately 600 KHz.

Reference 2 provides a detailed description of both technologies.

Both accelerometer types are referenced as those suited for pyroshock measurement in MIL STD 810G³.

In the following sequential sections of this paper are: (1) a description of the test environment, (2) identification of the accelerometer models tested, (3) a description of the instrumentation system, (4) top-level observations based on the accelerometer time-histories, (5) a description of the analysis performed with results, and (6) conclusions based on this analysis.

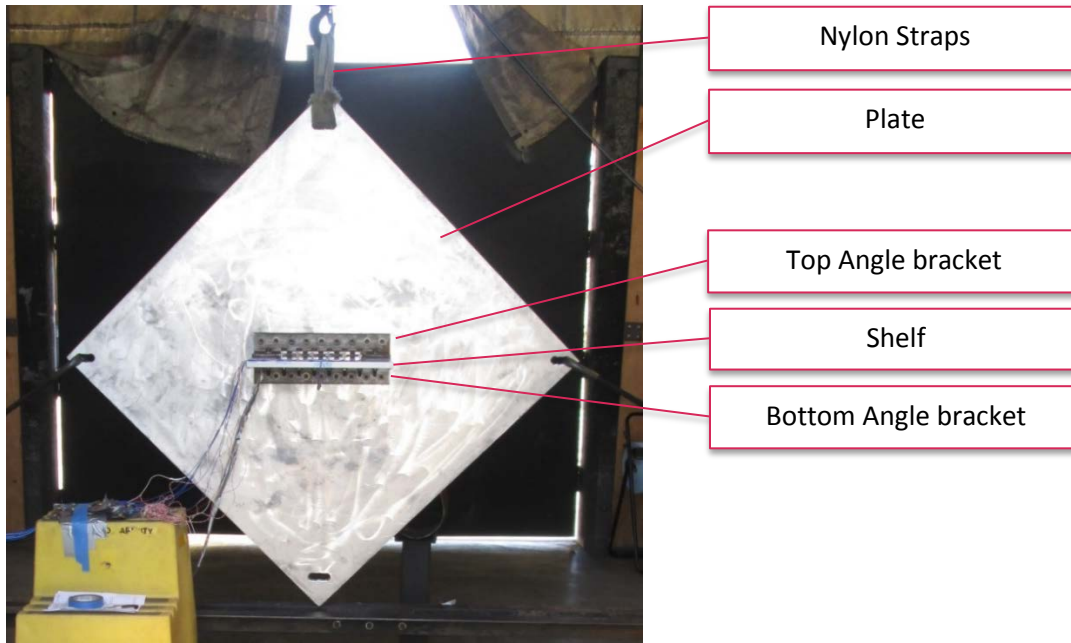
Test Environment

The 5 tests conducted (identified as Tests 2 - 6 since Test 1 was a simple hammer tap performed to verify setup) were pyrotechnic shocks using increasing levels of explosive.

The test fixture is shown in Figure 1. The primary structure was a *48 x 48 x 1 inch 6061* aluminum plate shown suspended with heavy nylon straps in the corners. An *18 x 12 x 0.75 inch 6061* aluminum shelf was mounted on the front side of the plate using two *3/8"* thick steel angle brackets. Each angle bracket was secured to the plate using nine *3/8-16* grade 8 bolts. The shelf was secured through both angle brackets using eight *3/8-16* grade 8 bolts. Bolt torque was checked before and after each test to assure consistency.

The accelerometers were mounted on 6061 aluminum 1" cube adaptor blocks, that were also secured to the shelf using *3/8-16* grade 8 bolts. The accelerometers were torqued before each test and checked afterwards against recommended values. The six blocks were oriented 45° normal to the shock axis in an attempt to keep the X & Y inputs approximately equivalent (Figure 2). The intent of this mounting orientation was to assess each accelerometer's performance in its sensing axis while it concurrently encountering a significant transverse acceleration in this same X-Y plane. Measurements discussed later also showed a significant Z-axis acceleration occurring.

The mounting surfaces of the plate and triaxial adaptor blocks were machined with a roughness of ≤ 8 Ra and a flatness of ≤ 0.001 ". Coupling grease was also applied to these surfaces to obtain optimal contact and shock transmissibility through each surface.



Nylon Straps

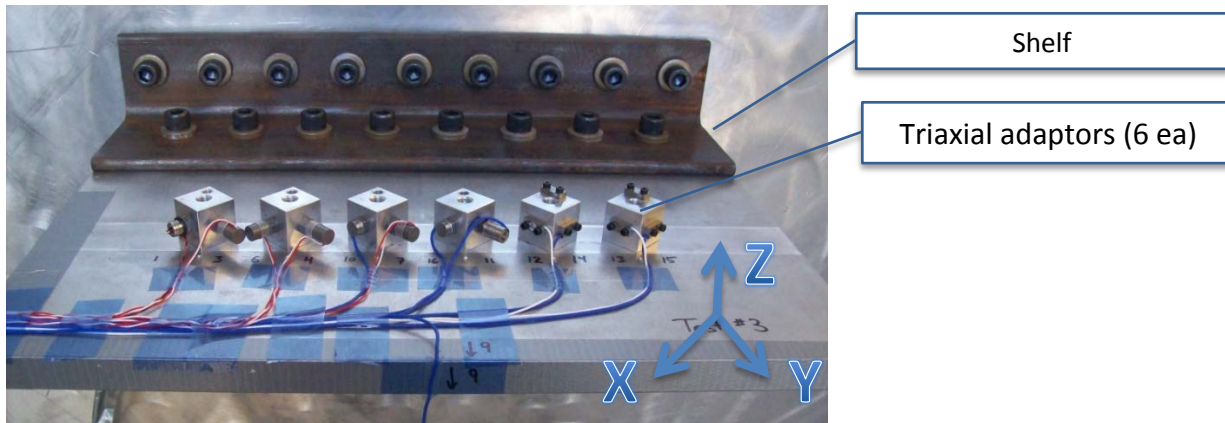
Plate

Top Angle bracket

Shelf

Bottom Angle bracket

Figure 1. Test Setup



Shelf

Triaxial adaptors (6 ea)

Figure 2. Mounting Blocks 1-6 (moving left to right) with Test Accelerometers (note: Z-axis accelerometers shown here were used in Test 6 only)

The explosives were mounted in an isosceles triangle configuration (Figure 3) on the back side of the plate, equal distances from the location of the center of the shelf. The excitation varied from three 2' coils of 15 grain/foot detonating cord to three 25' coils of 18 grain/foot detonating cord in five tests.

- Test 2: Three 2' coils of 15 grain/foot detonating cord
- Test 3: Three 5' coils of 15 grain/foot detonating cord
- Test 4: Three 10' coils of 15 grain/foot detonating cord
- Test 5: Three 20' coils of 15 grain/foot detonating cord
- Test 6: Three 25' coils of 18 grain/foot detonating cord

Increased explosive charge did not result in a proportional increase in shock amplitude. Test 6, consisting of three 25' coils of 18 grain/foot detonating cord, reached nominal peak acceleration amplitudes of only a factor of three (3) relative to Test 2. Two reasons are opined for this lack of proportionality. First, the explosive energy is largely

reflected from the rear surface of the plate. Second, with increased explosive quantity more energy was absorbed by inelastic plate deformation. Figure 4 is a picture (typical) of the plate deformation in front of one of the three coils of explosive after Test 6. By comparison, Test 2 resulted in almost no deformation to this same plate.

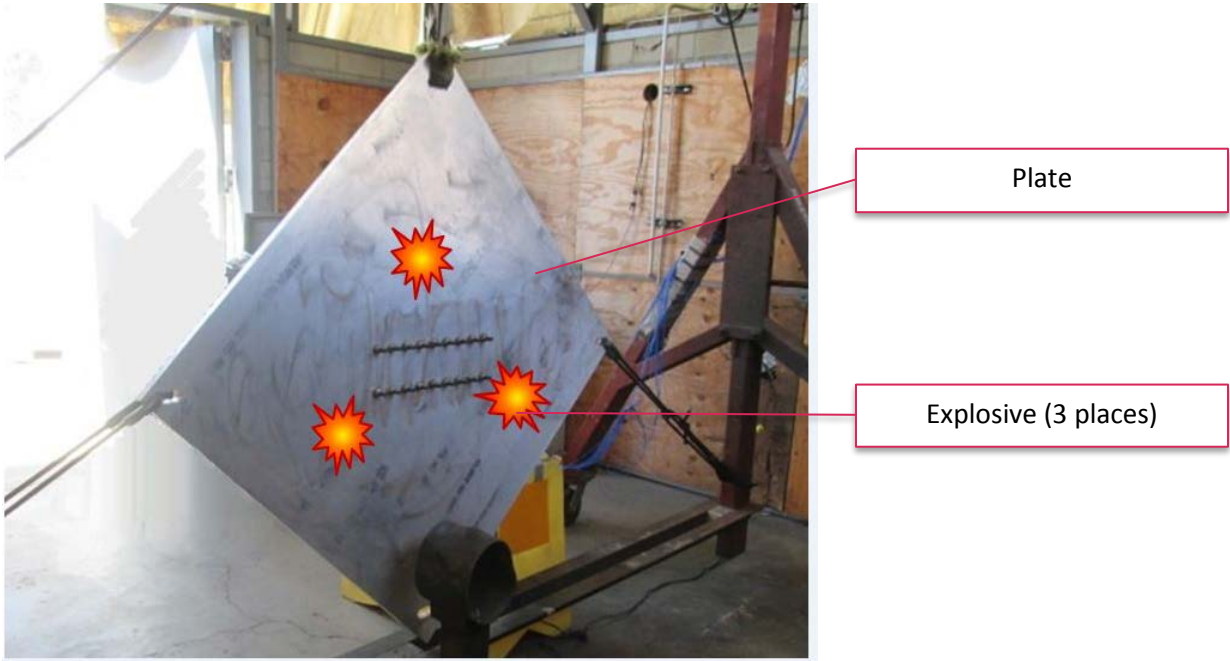


Figure 3. Explosive Loading Configuration Relative to Plate/Shelf

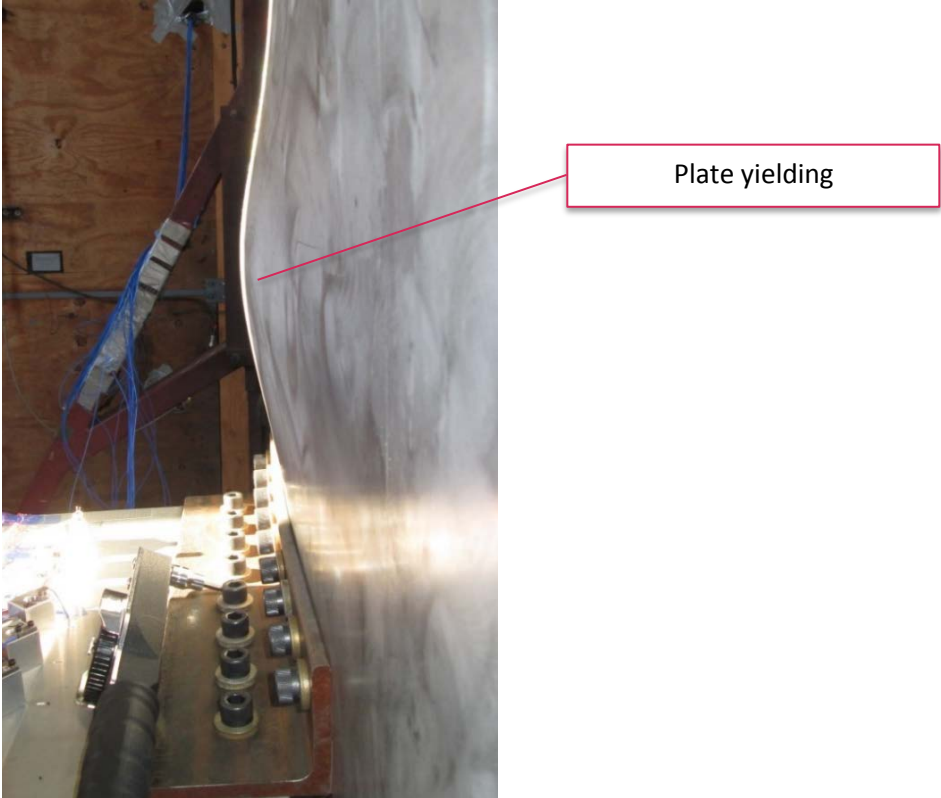


Figure 4. Local Plate Yielding

All of the accelerometers compared during these tests are listed below. They were randomly selected production models. All of them are commercially marketed for pyroshock measurement as defined in MIL STD 810G³.

For Tests 2 through 5 only the X (denoted Left) and Y (denoted Right) orientations on each block were actively occupied. Each block had 2 accelerometers located on it whose comparison was of particular interest to those supporting the testing. Figure 2, as noted, portrays the configuration for Test 6 during which additional active accelerometers were placed on the blocks in the Z (Vertical) direction. Recall Test 6 possessed the largest quantity of explosive loading. The below table details accelerometer placement for Test 2. In Test 3 the Block 2 Y accelerometer was switched to the Block 2 X position and the Y position then became occupied by a PCB Model 350B01. This X -Y configuration remained fixed for the remainder of all testing, i.e., Tests 3-6. Block 4 Y was occupied by a prototype accelerometer not commercially available so its results are not portrayed.

Manufacturer	Model	S/N	Technology	Block/Location	Channel Number
ENDEVCO	7255A	CF75	ISOL PE	1/Left	1
PCB	350B01	52322	ISOL PE	1/Right	3
ENDEVCO	7255A	CF78	ISOL PE	2/Left	2
PCB	350D02	50292	ISOL PE		6
PCB	350D02	50292	ISOL PE	2/Right	6
PCB	350B01	52323	ISOL PE		4
PCB	3501B	5805	MEMS	3/Left	10
PCB	350D02	50293	ISOL PE	3/Right	7
PCB	3501B	5806	MEMS	4/Left	16
N/A	N/A	N/A	N/A	4/Right	N/A
ENDEVCO	7270A	40423	MEMS	5/Left	12
PCB	3991B	3823	MEMS	5/Right	14
ENDEVCO	7280A	41800	MEMS	6/Left	13
PCB	3991B	3824	MEMS	6/Right	15

Note:

*Models 7255, 350D02, 350B01 are MIEF- IEPE technology
Models 3501B, 3991, 7270, 7280 are MEMS technology*

Prior to any pyro testing, the sensitivities of all of the accelerometers (including the effect of their 40' cables) were determined through a precise calibration process and these values were used in testing.

Instrumentation System Configuration

As noted, 40 feet of cable was required for each accelerometer to reach from the test bay to the test control and recording room. Each accelerometer type (MIEF-IEPE and MEMS) required different cables. After the signal from an accelerometer was transmitted through its cable, it passed through an appropriate amplifier and low pass filter and terminated into a data acquisition system.

Due to cable length the cable capacitance added additional filtering. This additional filtering was measured and considered in the design of the instrumentation system.

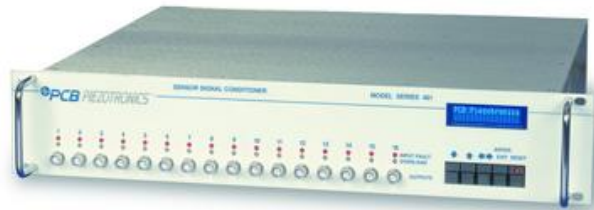
During testing, the cables were secured and adequate strain relief was provided (Figure 2). This assured the integrity of the cable and minimized the generation of any cable noise. Placebo accelerometers were also mounted, powered, and monitored on the test shelf to measure the instrumentation system noise floor.

When mounted, all MIEF- IEPE accelerometers were torqued to 4 ft lbs and all MEMS accelerometers were torqued to 8 in lbs. Mounting block surface preparation and cable tie down were described previously. Both accelerometer types had nominally flat frequency response to 10 KHz.

Above 10 KHz the frequency response of the isolated and internally filtered piezoelectric technologies is limited by the combination of their contained elastomeric material and their 2-pole internal electrical filter. 10 ma of drive current was provided to this accelerometer type to power the internal electronics and assure there were no additional frequency limitations below 10 KHz due to cable capacitance.

A PCB Y481A03 system was used to condition the isolated/filtered piezoelectric devices. MEMS accelerometers were conditioned with a PCB 482C27.

ICP©: PCB Y481A03 16



MEMS: PCB 482C27



Figure 5: Respective Signal Conditioning Used in all Calibration/Testing

Both signal conditioners had flat frequency response to 100 KHz. They were operated in the ac couple mode. For the MIEF- IEPE accelerometers the ac coupling removed the internal accelerometer bias voltage. The accelerometers themselves were -3 dB attenuated at nominally 2 Hz. For the MEMS accelerometers the ac coupling

removed bridge offset to enable symmetric operation around 0 volts. The ac coupling in both conditioners was low enough in frequency to assure data integrity above 10 Hz. Full scale amplifier output for both was 20 V pk - pk.

The conditioner gain was set to provide an expected maximum full scale signal of 4 V pk - pk (2.0 V 0 - pk). The gains were set to provide 7 KG 0 - pk full scale for Test 2, 14 KG for Test 3, and 21 KG for Tests 4, 5, and 6.

These ranges were conservatively selected to cover any expected transducer resonant response without amplifier saturation. Maximum signal full scale level recorded up to 10 KHz (Test 6) was nominally 15 KG. This level provided assurance that all accelerometers and analog signal conditioning operated within their linear range.

To allow direct comparison of accelerometer performance between types and models all signals needed to be frequency constrained to 10 KHz. The amplifier outputs were input to a Precision Filters PF-1UA-16FA-HP4F/LP4FP-Z low-pass 4-pole filter in "Pulse" mode. This filter provided excellent phase linearity and maintained amplitude response flat within 5% to 10 KHz. Signal content is attenuated by 95% (~ 26 dB at 94 KHz). This filter, plus filtering occurring due to capacitance in the cable run from the MEMS, attenuated any response at the resonances of the MEMS accelerometers by more than 50 dB. Thus, both MEMS and MIEF-IEPE channels could be ranged the same in terms of V/G.

The resulting signal was digitized with a DSPCon Piranha III data acquisition system. This system digitized the signal with a resolution of 16 bits over a range of +/- 2.5 volts and sampled at a rate of 1.2 million samples/second. Signal attenuation at the Nyquist frequency was so great as to eliminate any aliasing considerations. *In 2 instances the data acquisition system front end over ranged slightly and these records are identified and were processed but not evaluated.*

Macroscopic Data Observations in the Time Domain

This test provided a unique opportunity to compare a variety of sensor designs under crafted explosive pyrotechnic conditions. The following is provided as a global overview before a more intense data examination.

The time-domain plots when overlaying all sensors in each of the tests show a surprising degree of envelope uniformity. Viewed at high time resolution, however, the actual lack of correlation, and the difference between the responses of the various designs and locations is apparent. An example is shown in a view of the first 500 microseconds of Test #2 in Figure 6.

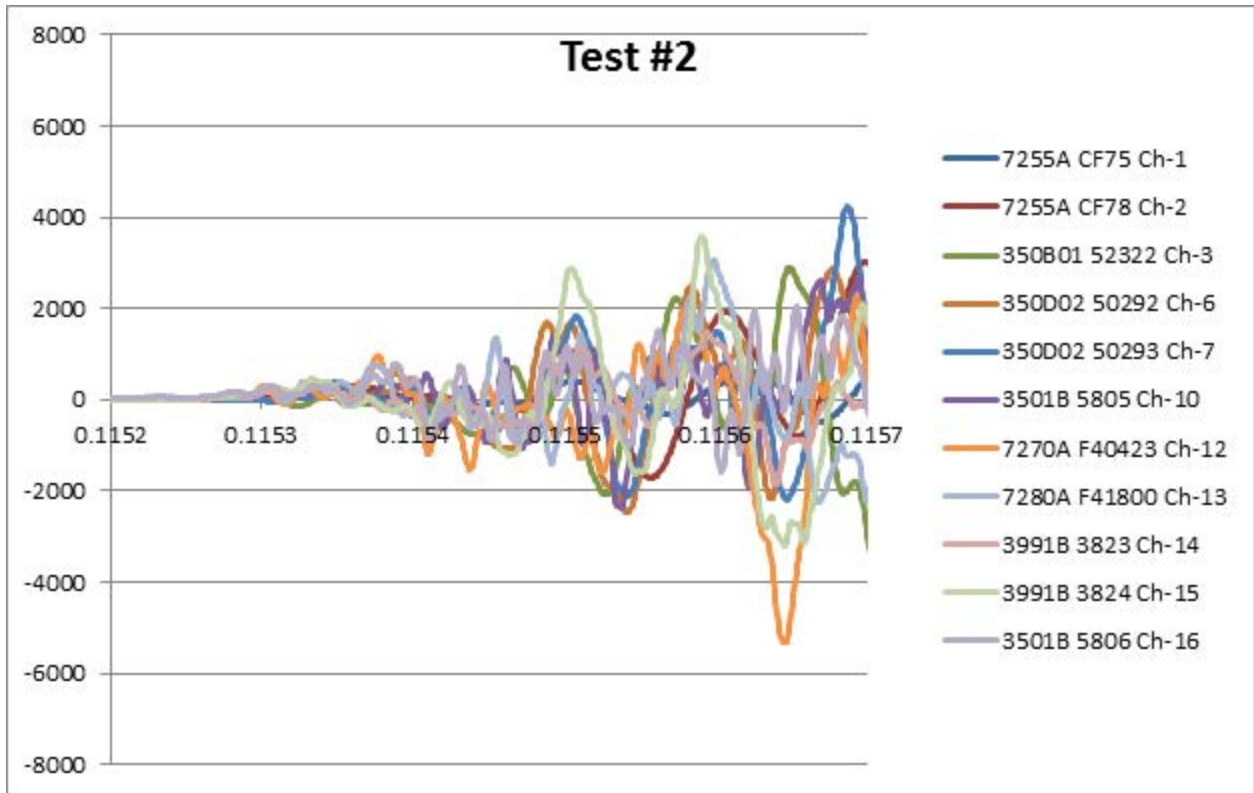


Figure 6: Initial 500 microseconds of Test #2 (G vs. time)

Figure 7 shows the results of averaging the left (X) and right (Y)-facing faces of the 45-degree angled blocks. During Test 6 additional sensors were attached on the tops of blocks (Z-axis), with sensitive axes normal to the plate. The average of the Z axis channels was very similar to the average of the Y axis for Test 6 (*the points are on top of one another*). Figure 7 provides an indication of the severity of the testing as suggested by the omnidirectional nature of the shock inputs encountered by the accelerometers.

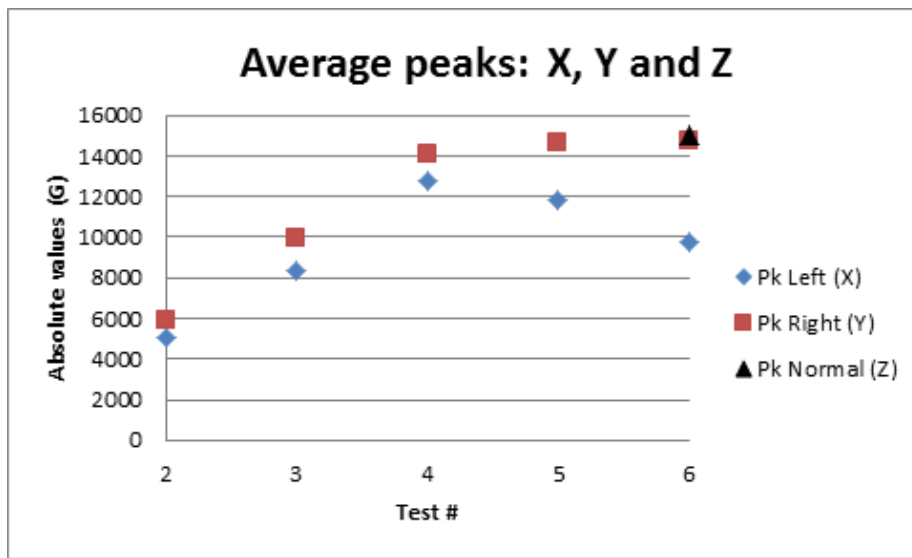


Figure 7: Averages of Peaks in the Three Axes (G vs. time)

Figures 8, 9, 10, 11, and 13 show general conformance of responses between accelerometers/locations for individual tests.

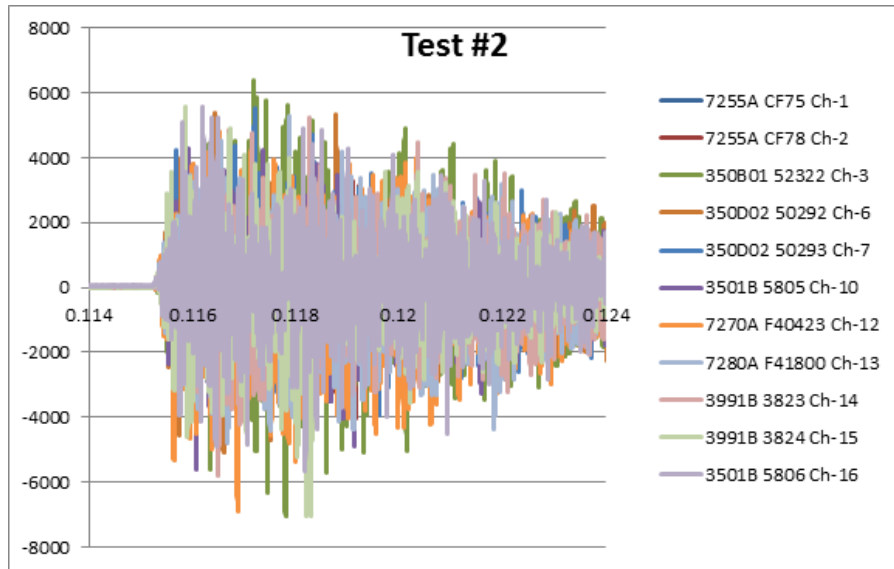


Figure 8: Time History of all Channels for Test #2 (G vs. time)

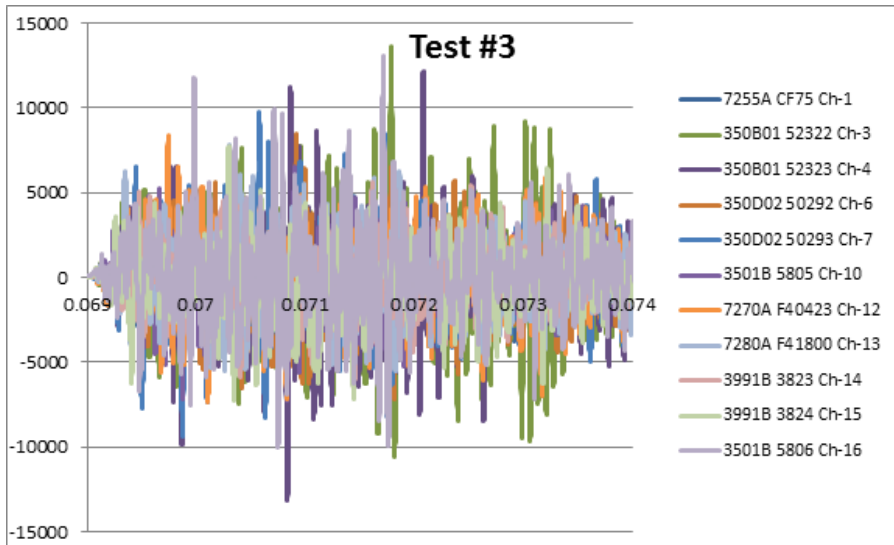


Figure 9: Time History of all Channels for Test #3 (G vs. time).

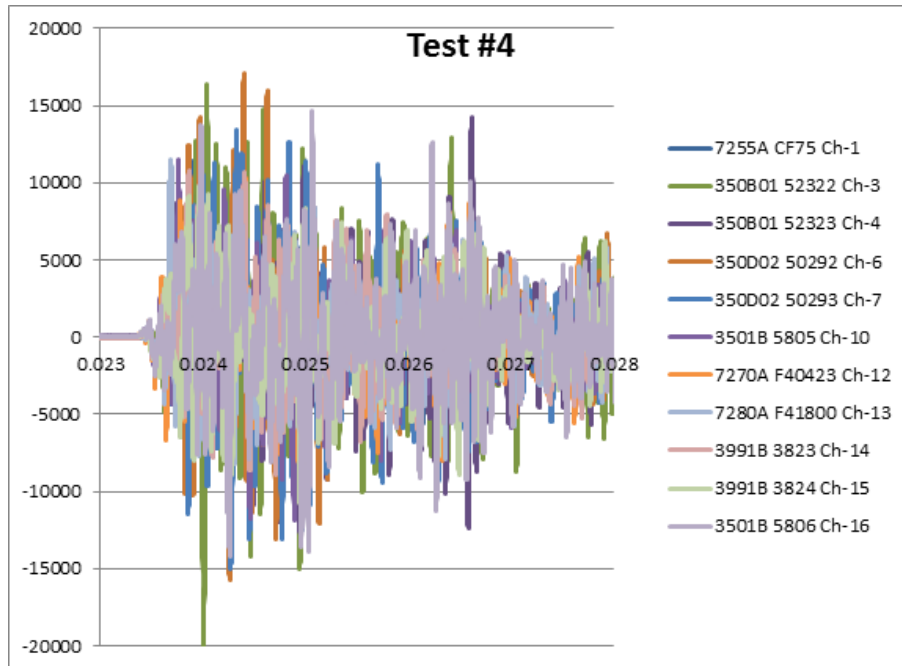


Figure 10: Time History of all Channels for Test #4 (G vs. time)

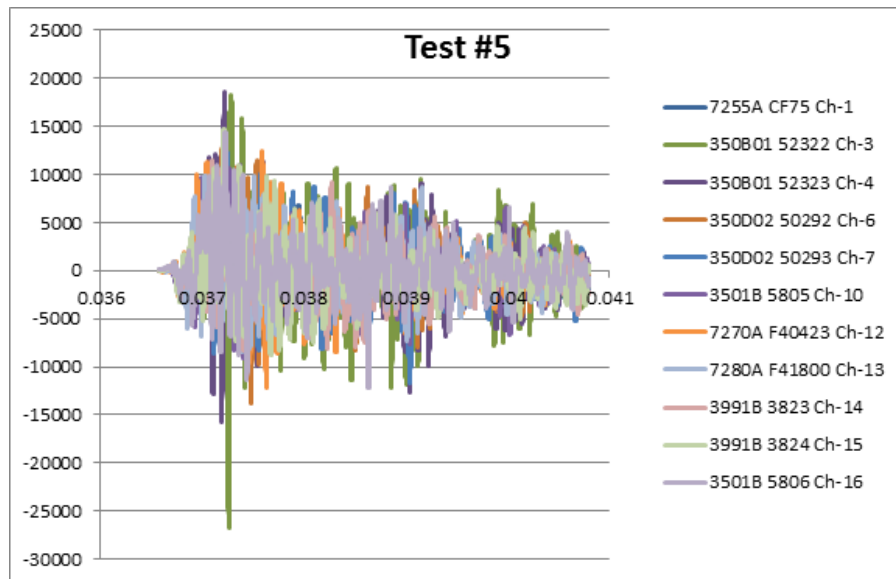


Figure 11: Time History of all Channels for Test #5 (G vs. time) .

The largest quantity of explosive was employed in Test #6. As noted, in this test an additional four accelerometers were placed in the Z axis on the top of the mounting blocks. As seen in Figure 12, they detected the shelf resonance, estimated at 940 Hz, with a pk-pk displacement of ~2 mm. All four sensors were tightly correlated after the second period of oscillation and provide additional credence to the omnidirectional nature of the input shock.

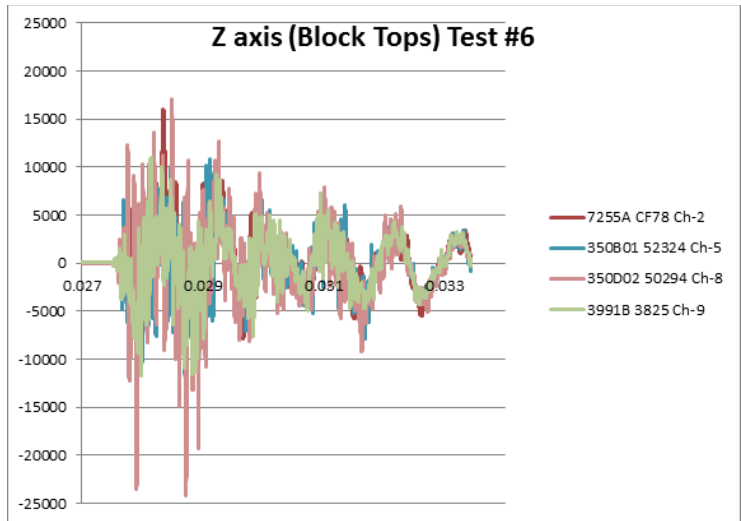


Figure 12: Time History of Z axis Sensors in Test #6 (G vs. time) .

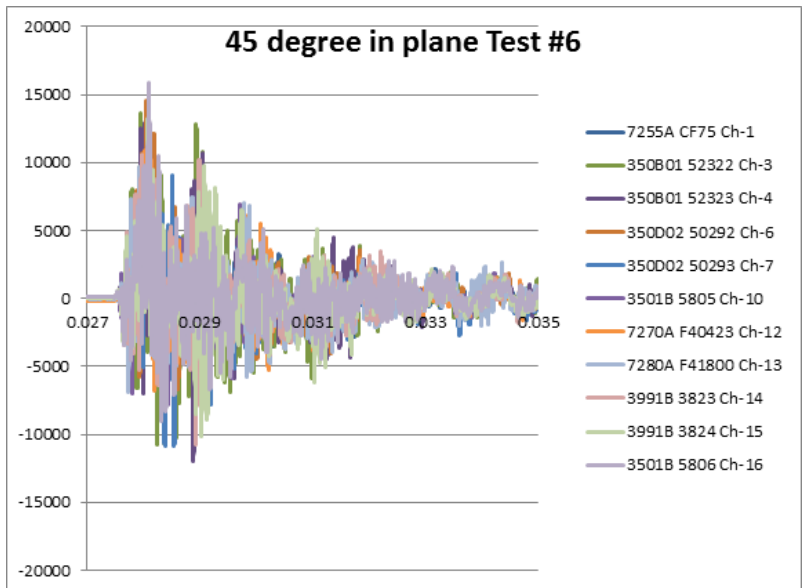


Figure 13: Time History of X and Y Axes Sensors in Test #6 (G vs. time)

Following are six plots decomposing Figure 13 by comparing the output of the two sensors on each of the six blocks (Test 6).

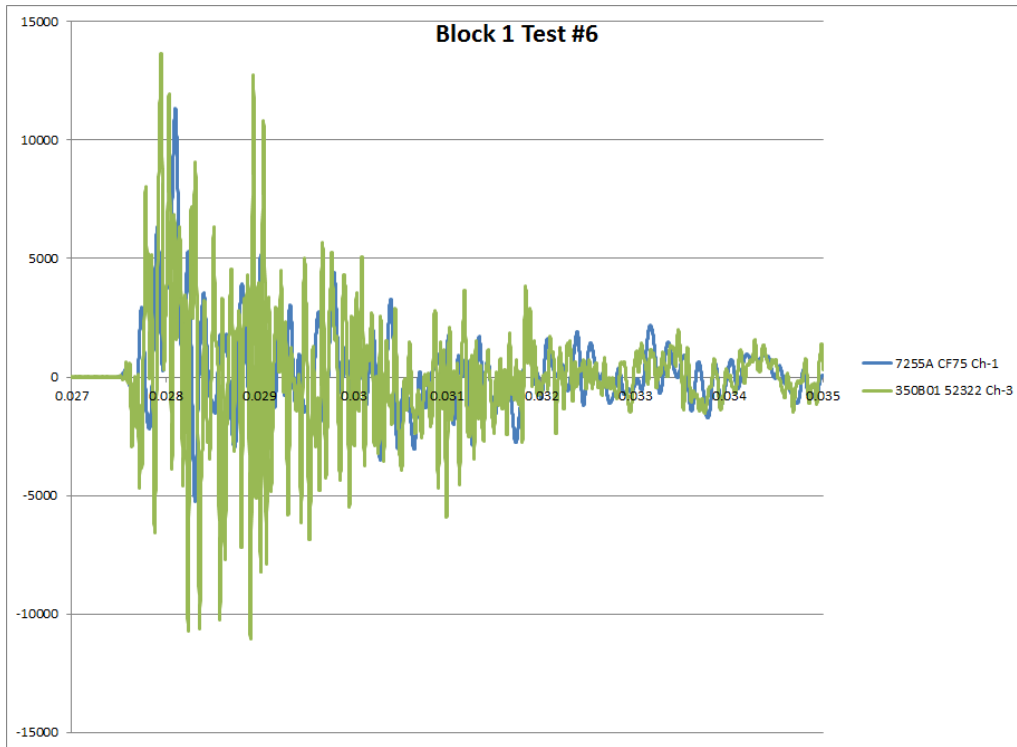


Figure14: Block 1 Test #6, S/N CF75 and 52322

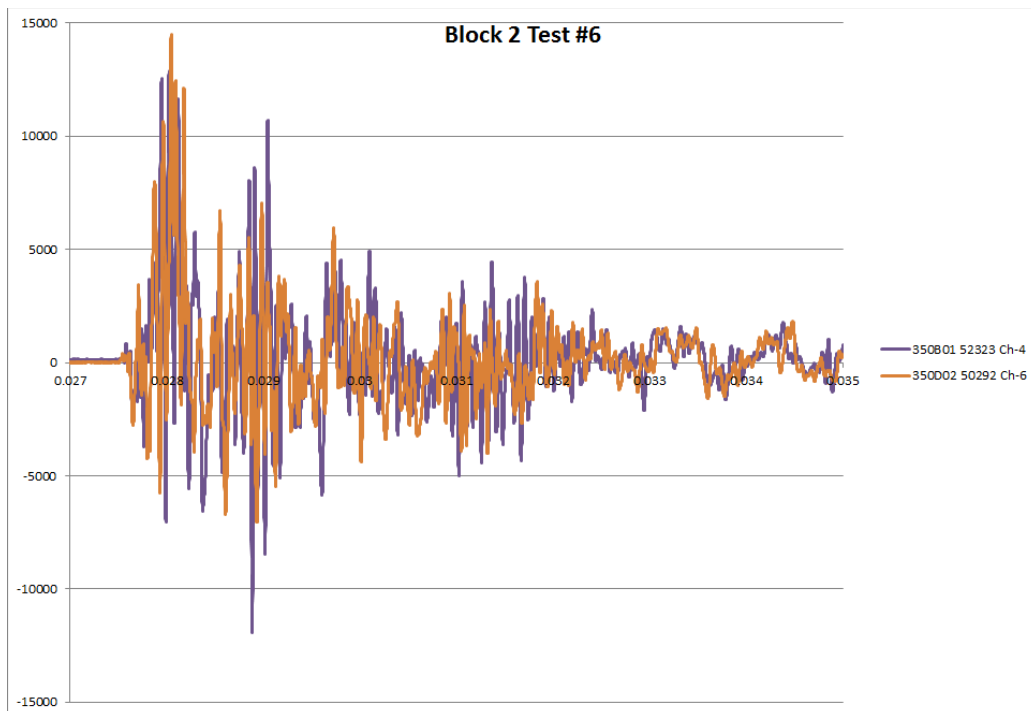


Figure15: Block 2 Test #6, S/N 52323 and 50292

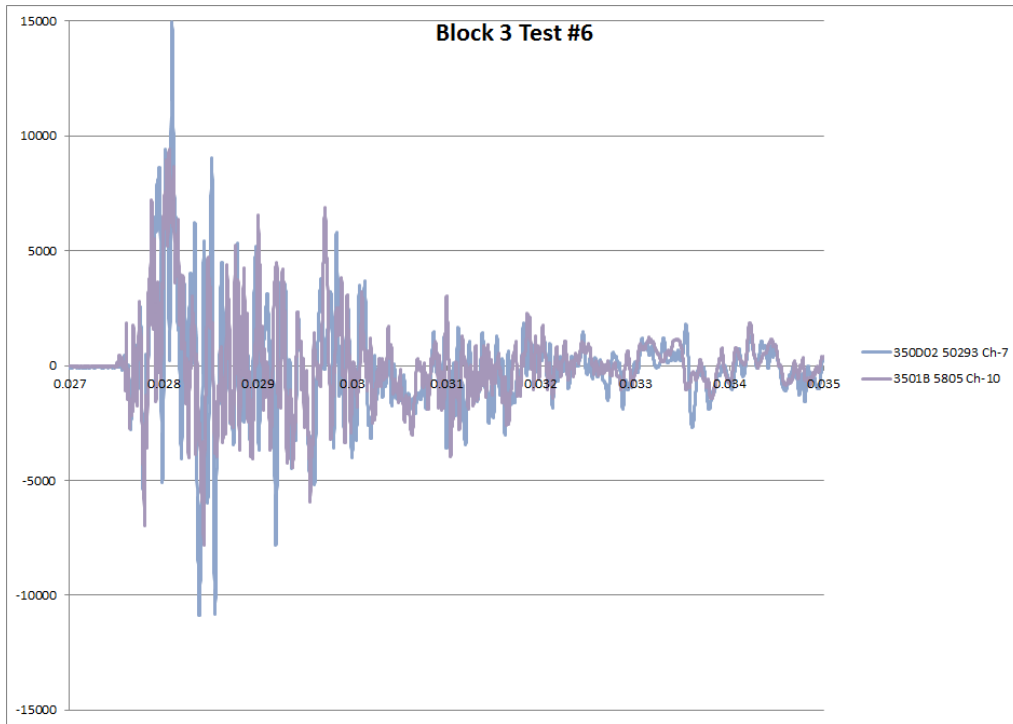


Figure 16: Block 3 Test #6, S/N 50293 and 5805

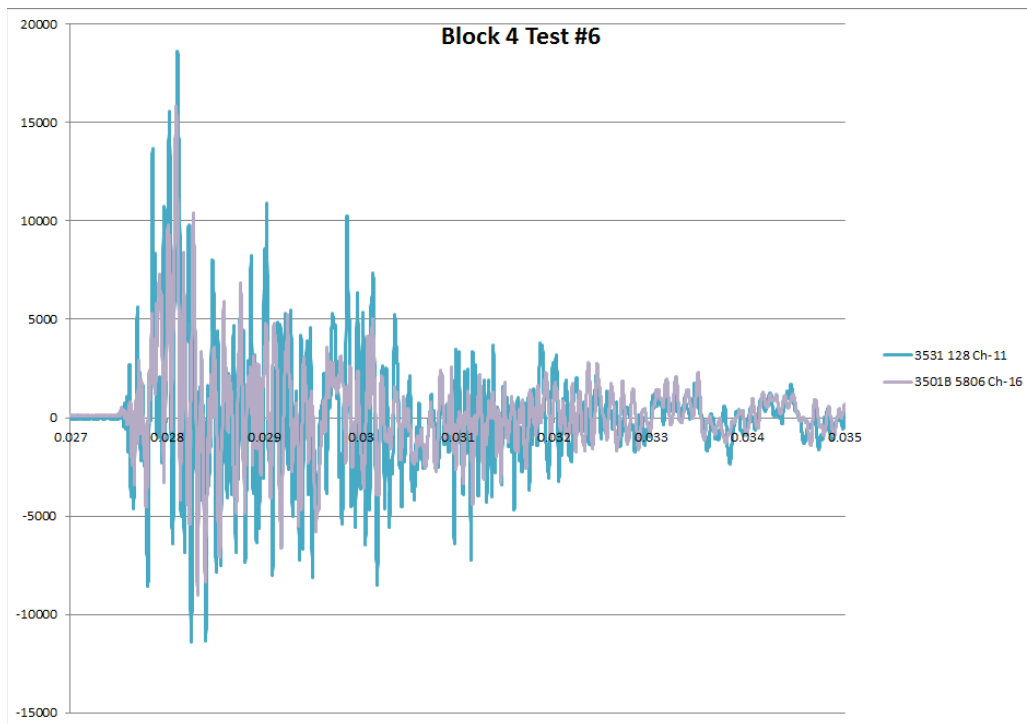


Figure 17: Block 4 Test #6, S/N 128 (prototype unit) and 5806

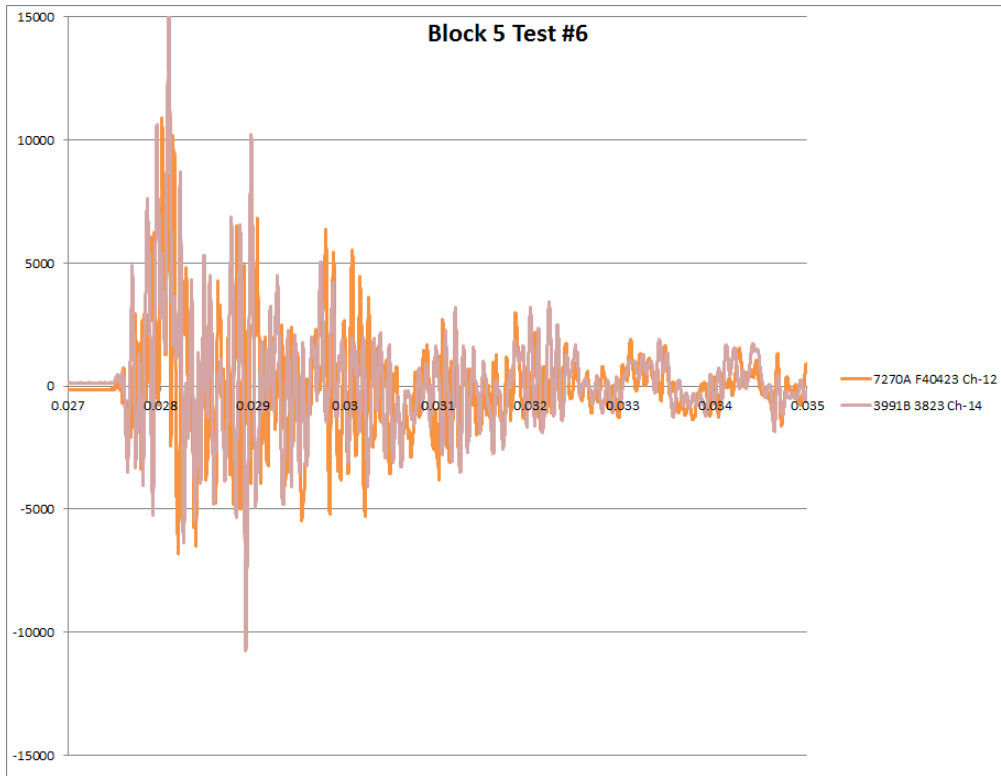


Figure 18: Block 5 Test #6, S/N F40423 and 3823

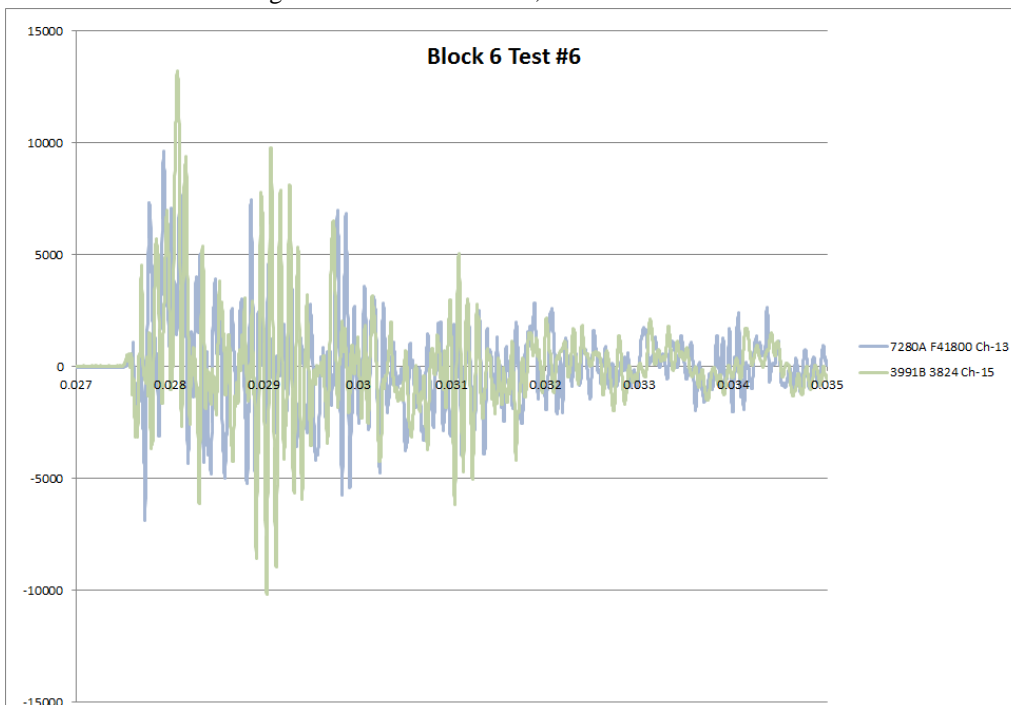


Figure 19: Block 6 Test #6, S/N F41800 and 3824

The preceding six time histories show that while some uniqueness exists, the X-Y accelerometers on each block generally follow the same profile.

Data Analysis and Results

The following procedure was used to analyze all of the data records:

1. A 0.3 second time history starting .001 seconds before the first evidence of motion was extracted from each experimental record.
2. The noise baseline immediately in front of the shock was averaged and the result was subtracted from the whole record.
3. The first 0.05 second of the record was plotted as shown upper left frame of Figure 20.
4. The integral (velocity) of the full period was calculated and the first 0.05 seconds plotted in the lower left frame.
 - a. The slope of the integral between .03 and .05 seconds was calculated by linear regression and is listed as the acceleration offset below the plots. This was then “normalized” by division by the peak-peak acceleration.
5. The Shock Response Spectrum (SRS) was calculated using the Smallwood algorithm⁵ from 10 Hz. to 10 KHz. for the full 300 millisecond period. The positive (solid) and negative (dotted) SRS curves are plotted in the upper right frame.
6. The RMS Fourier Spectrum was calculated for the full period and plotted from 10 Hz. to 100 KHz. in the lower right.

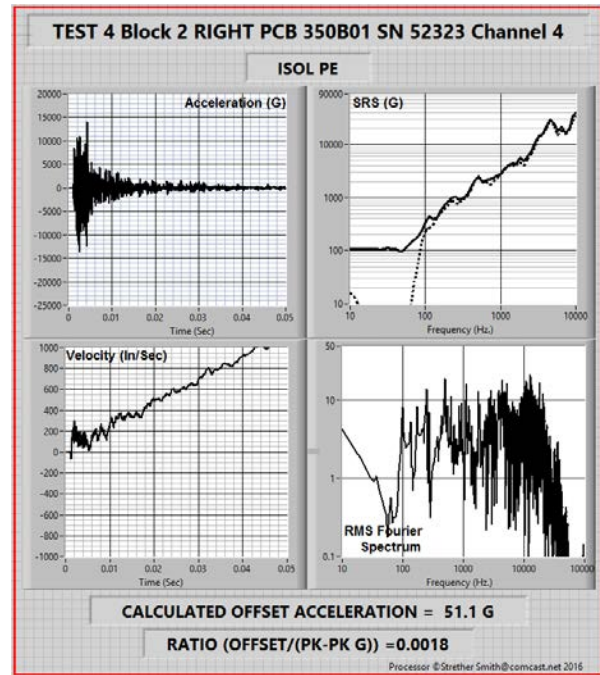


Figure 20. Typical Raw Data Analysis Plot

All of the test results are can be found in the Appendix in the back of the report.

Discussion of the Raw Results:

One of the remarkable findings of this study was that the acceleration offsets were as small as they are. For most of the records (all of the “good” accelerometers) the offsets were less than 0.25% of the Peak-to-Peak acceleration response.

However, even these tiny errors cause enormous discrepancies in the analyses that are normally performed.

For pyrotechnic shock tests, it is known that the velocity should be zero at the beginning and end of the test. Inspection of the velocity trace in Figure 20 (and in the Appendix for other channels) shows a very different result.

Any error in indicated velocity has serious consequences when assessing the damage potential of the measured signals. For example, the low-frequency portion of the acceleration Shock Response Spectrum (SRS) is seriously compromised by these experimental errors, even if they are very small.

The sensitivity of the SRS to these errors makes it a good diagnostic for assessing the tools that might be used to reduce the problem. Ideally, the SRS of a pyroshock waveform will have as a minimum these two characteristics:

- At low frequency (well below any structural mode activity) the slope of the SRS plotted in log-log form will be +2 (12dB/Octave).
- The positive and negative SRS results will be the same.

These SRS criteria, when combined with the fact that the velocity should be zero at the end of the test, give us an excellent set of criteria against which to assess any data correction attempt.

Correction Strategy:

Several methods have been proposed to reduce the effect of these experimental errors: High-pass filtering (References 6, 7) and wavelet correction (Reference 8).

This paper uses a third method based on the subtraction of velocity errors.

The strategy used is a refinement of the technique described in Reference 9. It uses the fact that we have a very good estimate of the velocity after the dynamics have settled down; the velocity must be very close to zero. Hence, any residual velocity must be an error.

The correction procedure is:

- Integrate the raw data to obtain velocity.
- Characterize the velocity error.
- Subtract the velocity error from the raw velocity.
- Differentiate the corrected velocity to find the corrected acceleration.

Of course, the challenge is to characterize the velocity error accurately. A correction curve, made up of three parts, is used:

- Zero, at the beginning of the transient.
- A low-order polynomial for the end (most of) the transient.
- A cubic spline to join the two.

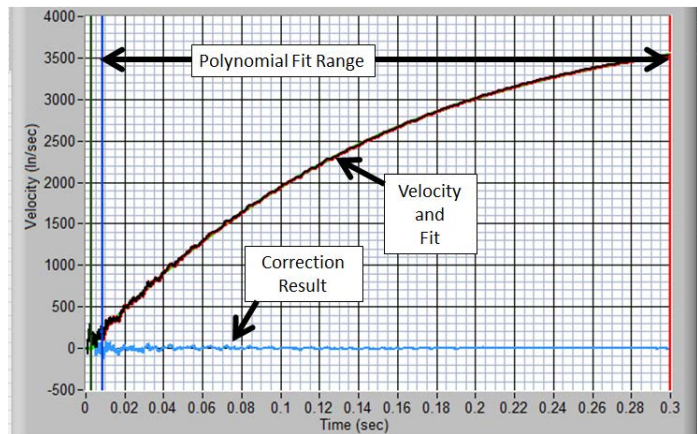


Figure 21. Full Analysis Period Fit

Figure 21 shows the correction for the full analysis time period. Details of the correction curve are shown in the expanded view of the shock start in Figure 22.

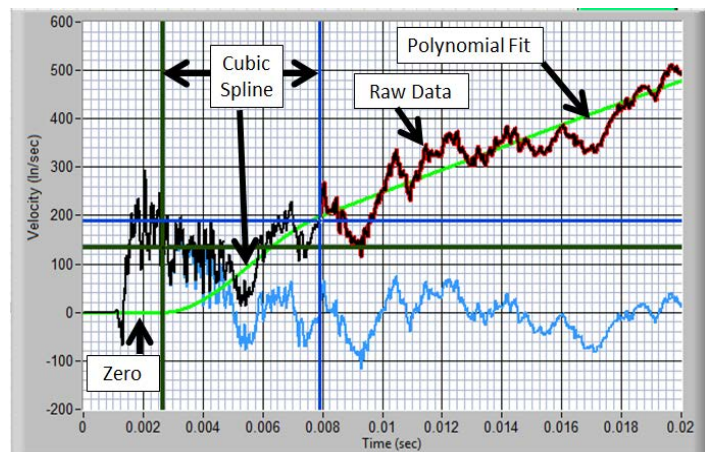


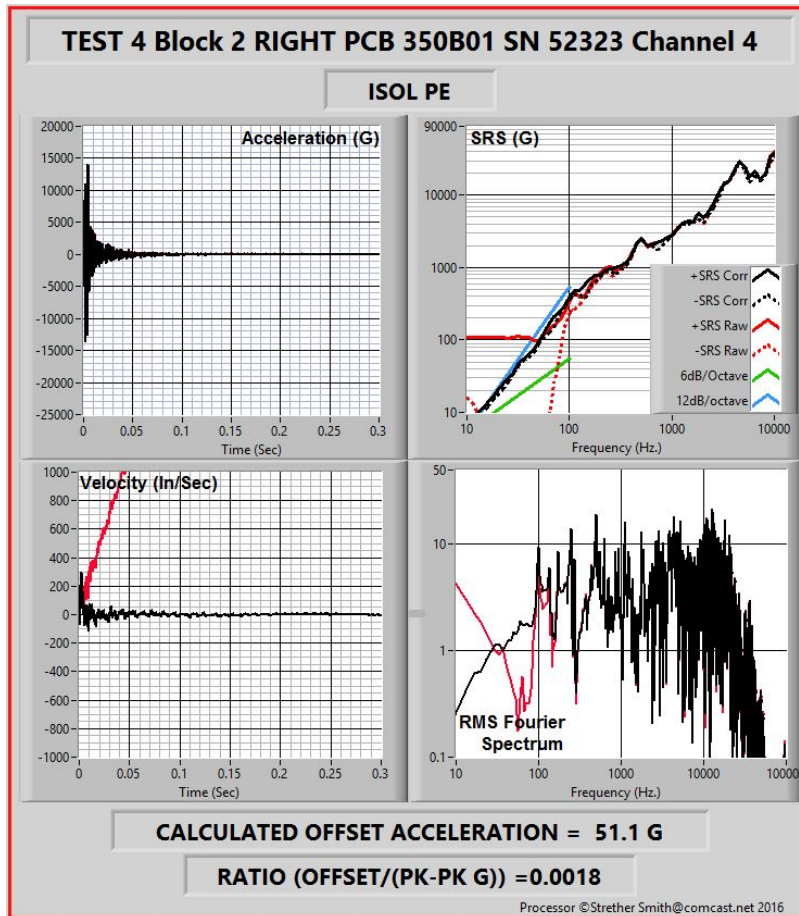
Figure 22. Analysis Curve Fit Detail

The “tuning” parameters are:

- The degree of the polynomial (usually 3rd or less).
- The start of the polynomial.
- The start of the spline.

In most cases, the parameters can be set once and used for all of the channels in a test. In a few cases, manual adjustment may be required.

The results for the example data set are shown in Figure 23.



It can be seen that:

- After the initial pulse, the velocity is very close to zero.
- The positive and negative SRS curves are essentially identical.
- The slope of the SRS at low frequency is very close to 12 dB/octave.

Examination of the results from all of the channels in the Appendix will show that the correction is generally very good for most of the channels.

Figure 23. Example Data Set Results

Tabulated Results:

As reported, five tests were performed and 11 channels of data were successfully recorded on every test. Eight (8) models of accelerometers were tested. Thus, on some tests a given model would be represented by more than one unit. On Test 2, two data channels were slightly over ranged at the input to the data acquisition system. To maintain objectivity in the analysis process, these two channels were denoted as CHANNEL SATURATION even though the amount of over ranging was slight. The response of one unit in Test 5 was intermittent after the shock ended. It was denoted INTERMITTENT. Its time history also appeared a bit unusual.

As a minimum, an assessment of test results can consider the calculated SRSs, the Fourier spectra of the signals, the symmetry of the positive and negative SRSs, and the resultant measured zero offsets. Some of these considerations are interrelated. In trying to perform an impartial assessment the authors decided they could only achieve consensus agreement using the criteria of GOOD, BAD, and QUESTIONABLE for each recorded data channel. ALL authors had to collectively agree to make a definitive call.

Recognizing that this test was coordinated by PCB Piezotronics Inc., and involved a competitor's accelerometers, independent consultants were invited to participate. In addition, every recorded and processed test result is presented in the Appendix (55 records) for viewing and assessment by other interested parties.

PYROSHOCK ACCELEROMETER EVALUATION RESULTS									
Manufacturer	Model	S/N	Technology	Block/Location	Test 2	Test 3	Test 4	Test 5	Test 6
ENDEVCO	7255A	CF75	ISOL PE	1/Left	BAD	BAD	BAD	BAD	BAD
PCB	350B01	52322	ISOL PE	1/Right	CHANNEL SATURATED	GOOD	GOOD	GOOD	GOOD
ENDEVCO	7255A	CF78	ISOL PE	2/Left	BAD				
PCB	350D02	50292	ISOL PE			GOOD	GOOD	GOOD	GOOD
PCB	350D02	50292	ISOL PE	2/Right	GOOD				
PCB	350B01	52323	ISOL PE			GOOD	GOOD	GOOD	GOOD
PCB	3501B	5805	MEMS	3/Left	BAD	BAD	GOOD	GOOD	GOOD
PCB	350D02	50293	ISOL PE	3/Right	GOOD	GOOD	GOOD	GOOD	GOOD
PCB	3501B	5806	MEMS	4/Left	BAD	BAD	GOOD	GOOD	GOOD
				4/Right	*****	*****	*****	*****	*****
ENDEVCO	7270A	40423	MEMS	5/Left	GOOD	QUESTIONABLE	GOOD	GOOD	GOOD
PCB	3991B	3823	MEMS	5/Right	QUESTIONABLE	QUESTIONABLE	GOOD	GOOD	GOOD
ENDEVCO	7280A	41800	MEMS	6/Left	GOOD	GOOD	GOOD	INTERMITTENT	BAD
PCB	3991B	3824	MEMS	6/Right	CHANNEL SATURATED	QUESTIONABLE	GOOD	GOOD	GOOD

Conclusions

- An evaluation of the performance of eight (8) different models of accelerometers in severe pyroshock environments has been planned, executed, and analyzed. This effort was characterized by:
 - Omnidirectional shock inputs to tens of thousands of Gs of almost equal magnitudes in all directions,
 - Matched transfer characteristics on all data channels with verified flat amplitude and linear phase to 10 KHz (the upper normal SRS analysis frequency),
 - Distortion free data return on 53 of 55 recorded data channels, and a
 - Consistent data analysis process.
- Analysis indicates that the MIEF-IEPE type shock accelerometers provided GOOD results and performed at least as well as the MEMS type in all testing, with the exception of two units characterized as BAD via nonlinear behavior consistent with prior work as described in Reference 2 (see Tabulated Results, Endevco Model 7255).
- Given the potential sources of zero shift in acceleration records *identified in the report Introduction*, test results were much better than anticipated. Based on the “as recorded” data, a maximum acceleration offset (i.e., zero shift) of less than 0.25% referenced to the pk-pk value was recorded across all results marked “GOOD” (see Appendix).

Since all test results are published in the back of this report, interested individuals can draw their own comparative conclusions.

These experiments showed that modern versions of accelerometers using both MIEF-IEPE and MEMS technology provided excellent results for excitations encountered in high-level pyrotechnic testing.

This finding should be recognized in future test specifications and standards.

References

1. Dosch, Jeffrey, Lin Jing, "Hopkinson Bar Acceptance Testing for Shock Accelerometers", Sound and Vibration, February 1999.
2. Agnello, Anthony, Dosch, Jeffrey, Metz, Robert, Sill, Robert, Walter, Patrick, "Acceleration Sensing Technologies for Severe Mechanical Shock", Sound and Vibration, pp. 9-18, February 2014.
3. MIL-STD-810G, DEPARTMENT OF DEFENSE TEST METHOD STANDARD: ENVIRONMENTAL ENGINEERING CONSIDERATIONS AND LABORATORY TESTS (31 OCT 2008).
4. Walter, Patrick L., "Lessons learned in applying accelerometers to nuclear effects testing", Shock and Vibration, (14), pp. 1-11, 2007.
5. Smallwood, David: "An Improved Recursive Formula for Calculating Shock Response Spectra" 51st Shock and Vibration Bulletin, 1980.
6. Smallwood, David O., and Jerome S. Cap, "Salvaging Pyrotechnic Data with Minor Overloads and Offsets," *Journal of the Institute of Environmental Sciences and Technology*, Vol. 42, No. 3, pp. 27-35.
7. Smith, Strether, and Bill Hollowell, "Techniques for the Normalization of Shock Data," *Proceedings of the 62nd Shock and Vibration Symposium*, Springfield VA, 1991.
8. An improved wavelet correction for zero shifted accelerometer data, Timothy S. Edwards, Shock and Vibration 10, 159-167, IOS Press, 2003.
9. Smith, Strether, TEST DATA ANOMALIES—When Tweaking's OK, Sensors Magazine, December 2003.

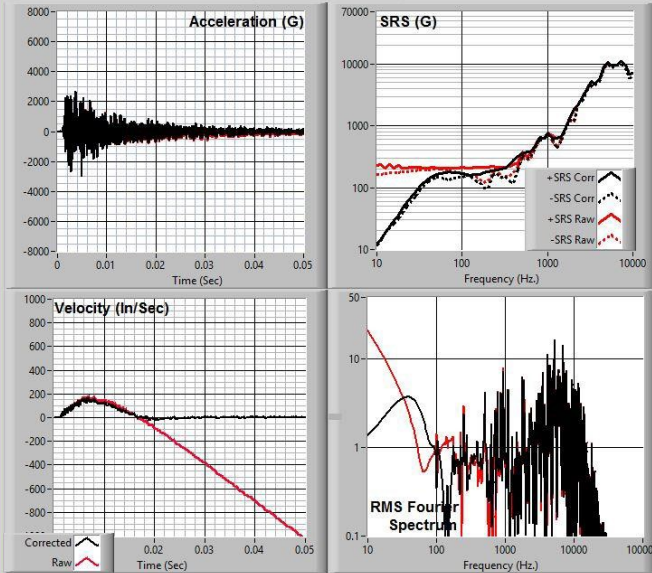
Acknowledgement

Appreciation is expressed to Mr. Bob Metz, PCB, for supporting this activity and maintaining hands off to allow an objective data analysis process. Appreciation is similarly expressed to Mr. Lou Zagst, PCB, for coordination of the test interface with NTS. Special gratitude is provided to Mr. John Czajkowski for permitting access to National Test Systems (NTS) excellent test facility in Santa Clarita, CA. Mr. Steve Fulton and Mr. Dave Williams are awarded many thanks for their dedicated support during this true ordnance pyroshock test series.

APPENDIX

TEST 2 Block 1 LEFT ENDEVCO 7255 SN CF75 Channel 1

ISOL PE



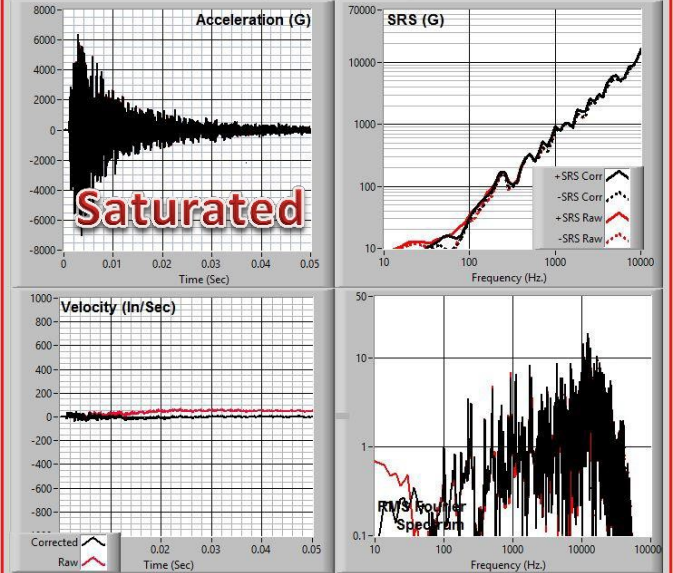
CALCULATED OFFSET ACCELERATION = -83.5 G

RATIO (OFFSET/(PK-PK G)) = -0.0147

Processor ©Strether Smith@comcast.net 2016

TEST 2 Block 1 RIGHT PCB 350B01 SN 52322 Channel 3

ISOL PE



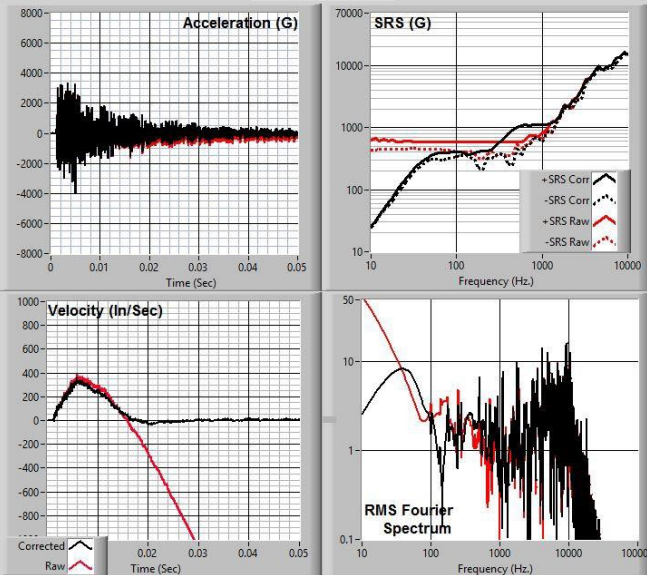
CALCULATED OFFSET ACCELERATION = -1.0 G

RATIO (OFFSET/(PK-PK G)) = -0.0001

Processor ©Strether Smith@comcast.net 2016

TEST 2 Block 2 LEFT ENDEVCO 7255 SN CF78 Channel 2

ISOL PE



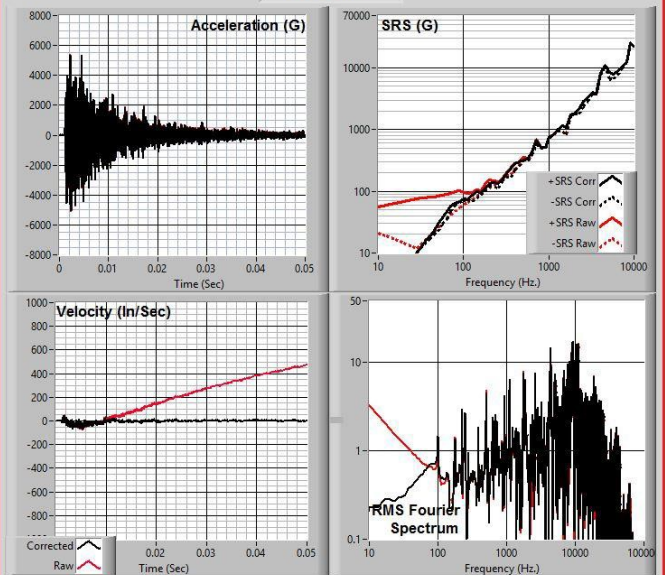
CALCULATED OFFSET ACCELERATION = -226.1 G

RATIO (OFFSET/(PK-PK G)) = -0.0307

Processor ©Strether Smith@comcast.net 2016

TEST 2 Block 2 RIGHT PCB 350D02 SN 50292 Channel 6

ISOL PE



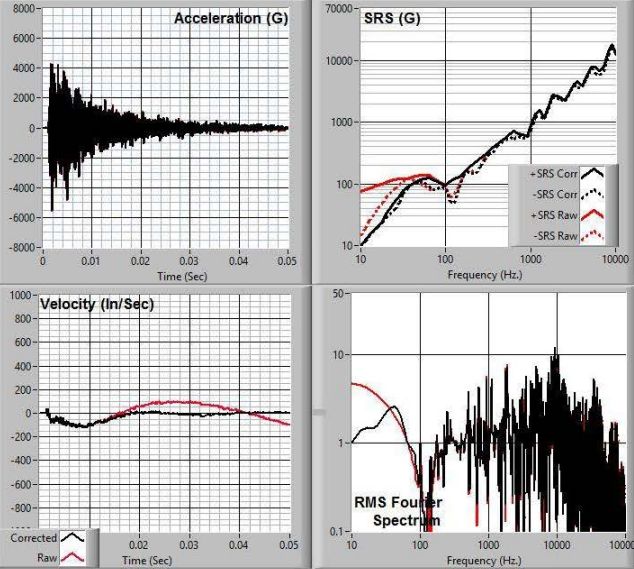
CALCULATED OFFSET ACCELERATION = 25.8 G

RATIO (OFFSET/(PK-PK G)) = 0.0025

Processor ©Strether Smith@comcast.net 2016

TEST 2 Block 3 LEFT PCB 3501B SN 5805 Channel 10

MEMS



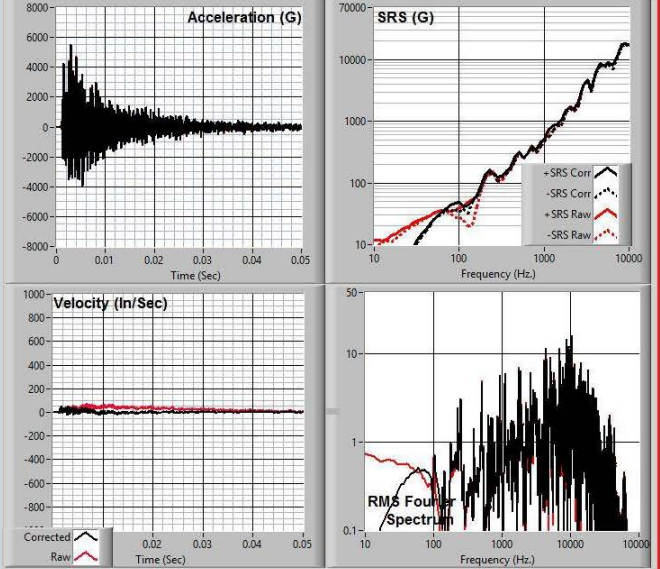
CALCULATED OFFSET ACCELERATION = -25.8 G

RATIO (OFFSET/(PK-PK G)) = -0.0026

Processor ©Strether Smith@comcast.net 2016

TEST 2 Block 3 RIGHT PCB 350D02 SN 50293 Channel 7

ISOL PE



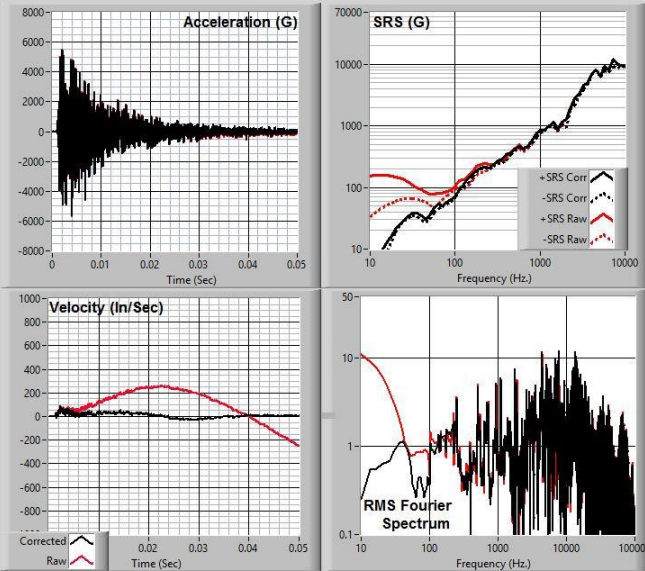
CALCULATED OFFSET ACCELERATION = -2.5 G

RATIO (OFFSET/(PK-PK G)) = -0.0003

Processor ©Strether Smith@comcast.net 2016

TEST 2 Block 4 LEFT PCB 3501B SN 5806 Channel 16

MEMS



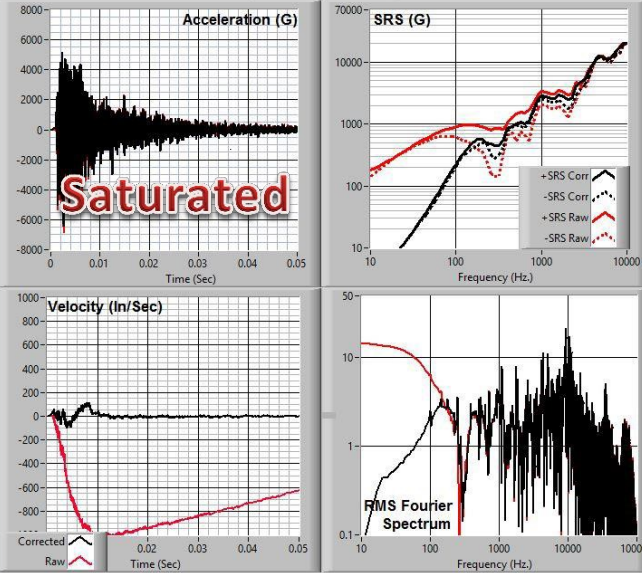
CALCULATED OFFSET ACCELERATION = -58.4 G

RATIO (OFFSET/(PK-PK G)) = -0.0052

Processor ©Strether Smith@comcast.net 2016

TEST 2 Block 5 LEFT ENDEVCO 7270 SN 40423 Channel 12

MEMS



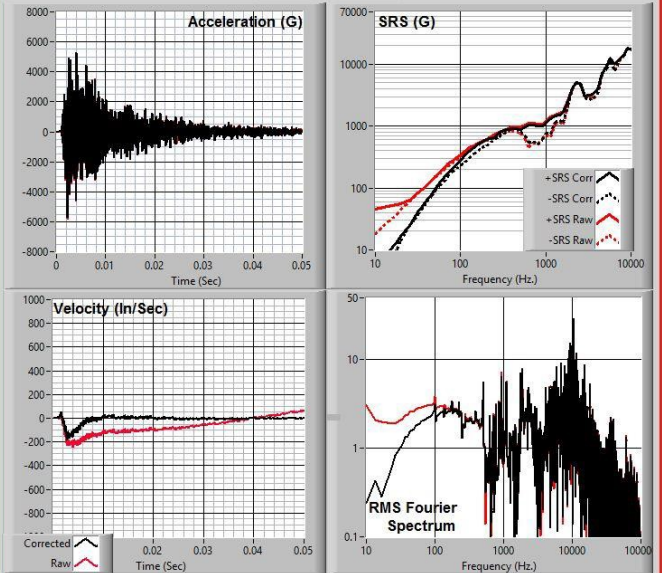
CALCULATED OFFSET ACCELERATION = 28.1 G

RATIO (OFFSET/(PK-PK G)) = 0.0024

Processor ©Strether Smith@comcast.net 2016

TEST 2 Block 5 RIGHT PCB 3991 SN 3823 Channel 14

MEMS



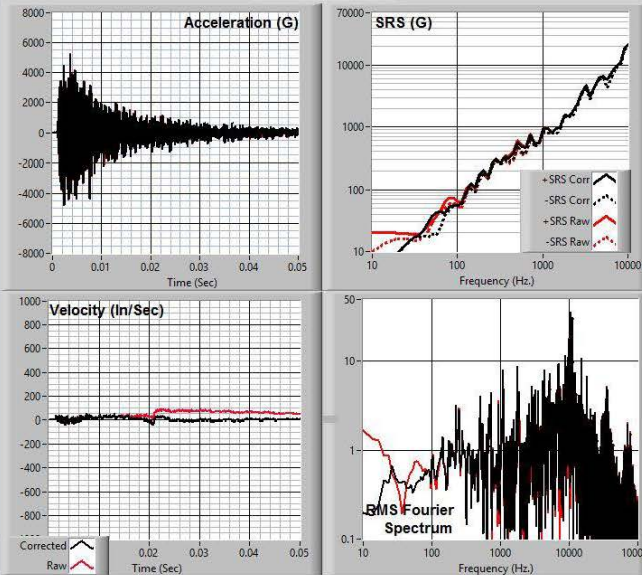
CALCULATED OFFSET ACCELERATION = 16.0 G

RATIO (OFFSET/(PK-PK G)) = 0.0014

Processor ©Strether Smith@comcast.net 2016

TEST 2 Block 6 LEFT ENDEVCO 7280 SN 41800 Channel 13

MEMS



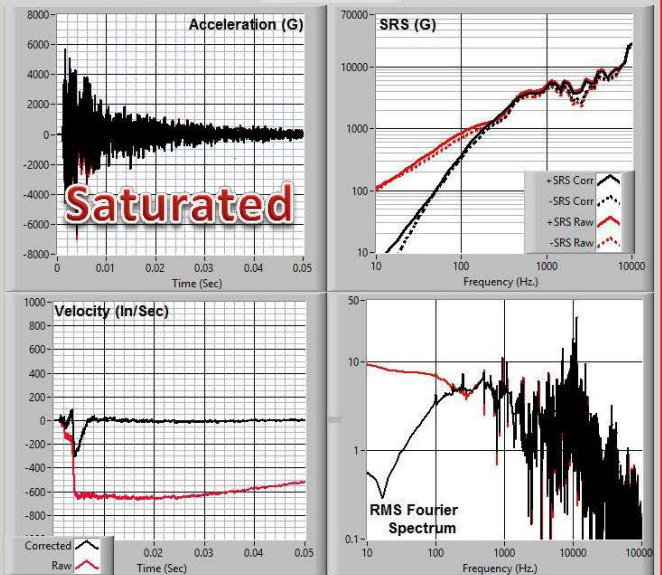
CALCULATED OFFSET ACCELERATION = -3.5 G

RATIO (OFFSET/(PK-PK G)) = -0.0003

Processor ©Strether Smith@comcast.net 2016

TEST 2 Block 6 RIGHT PCB 3991 SN 3824 Channel 15

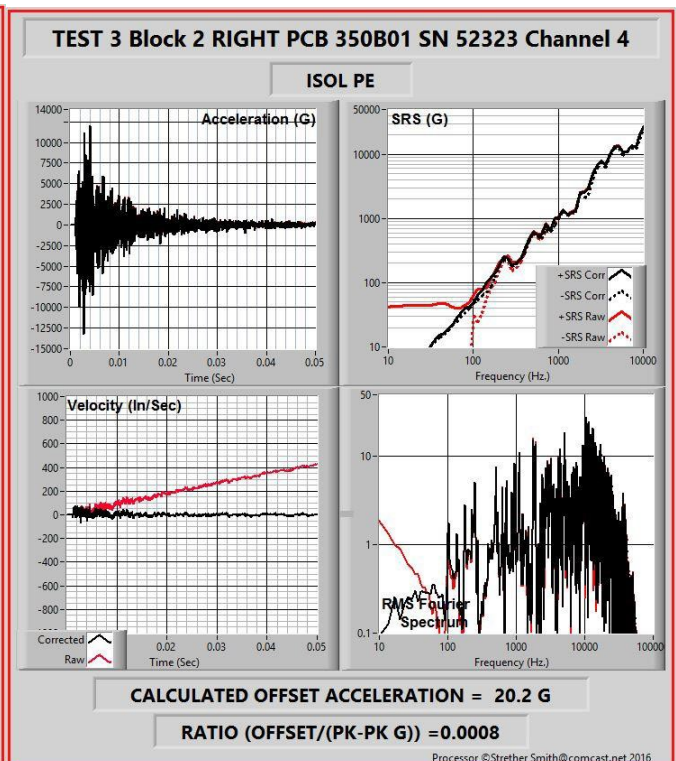
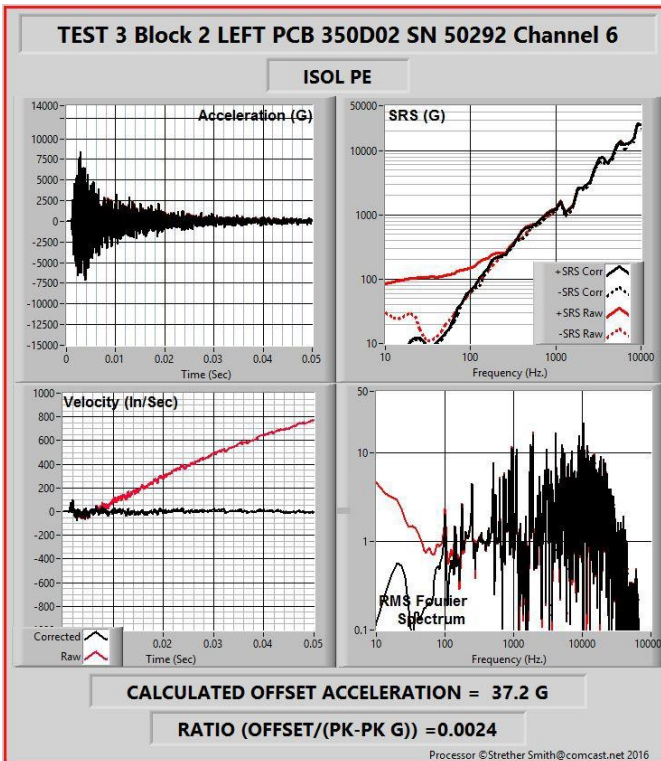
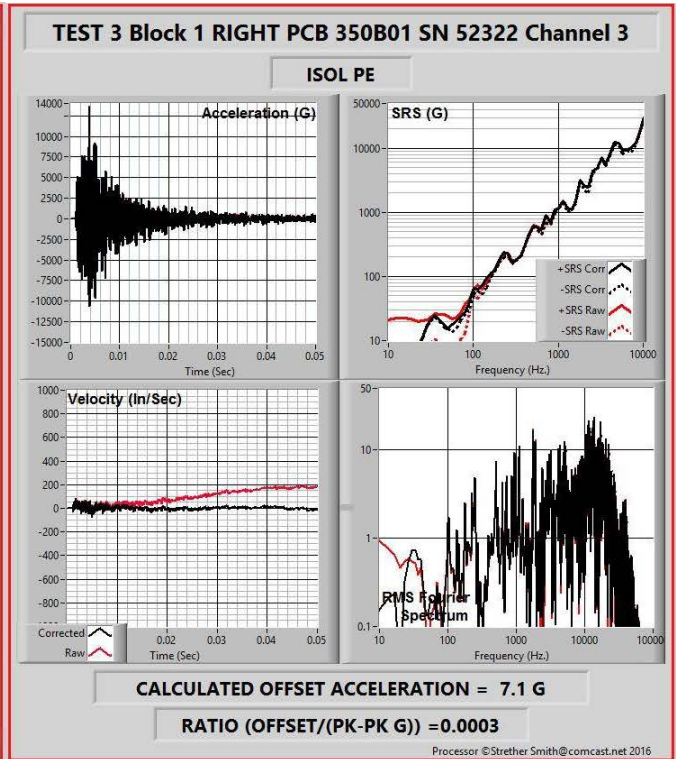
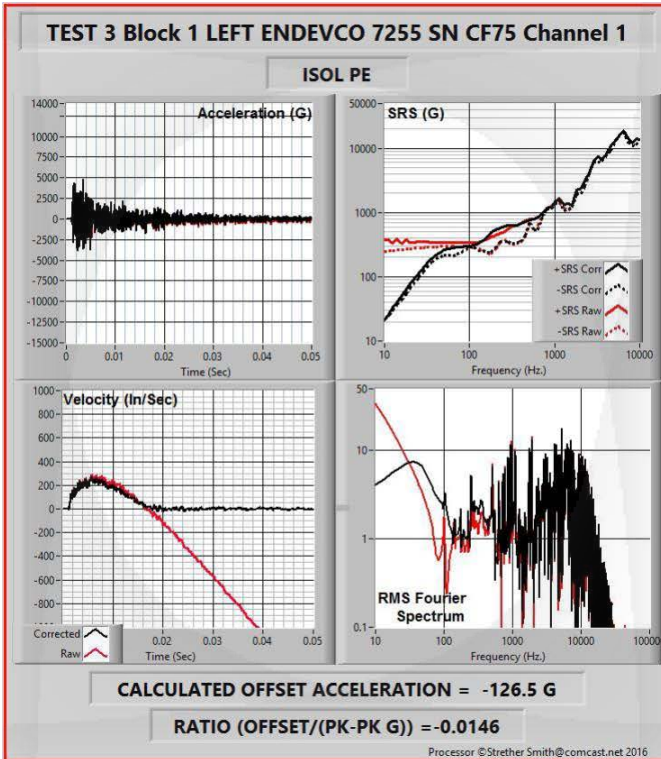
MEMS

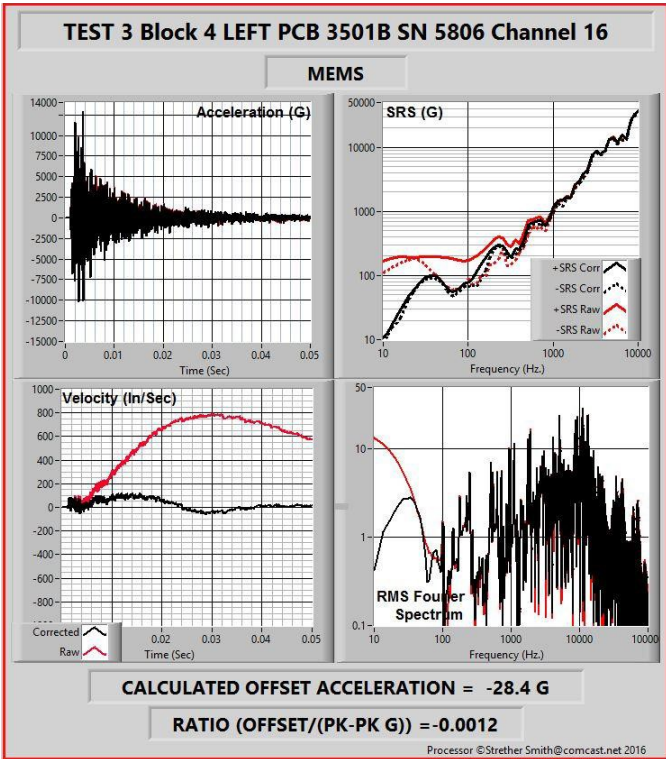
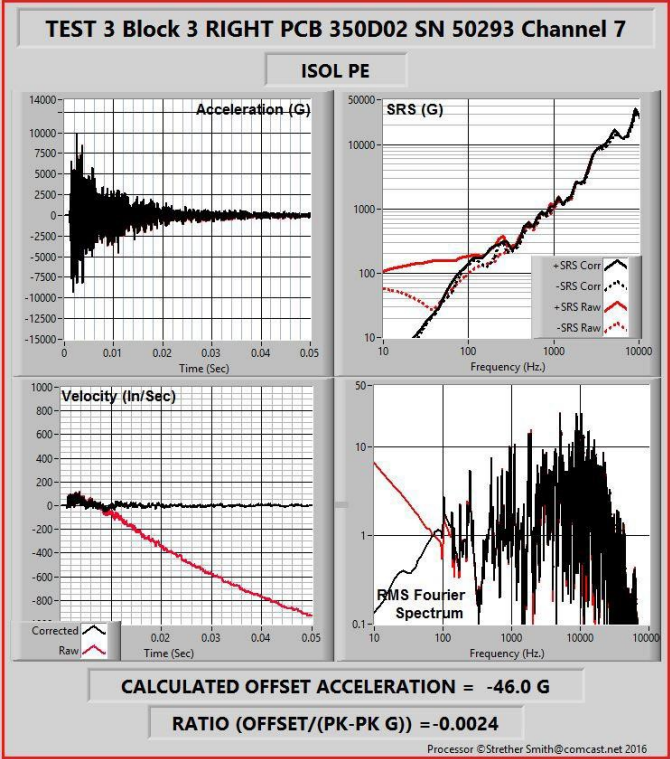
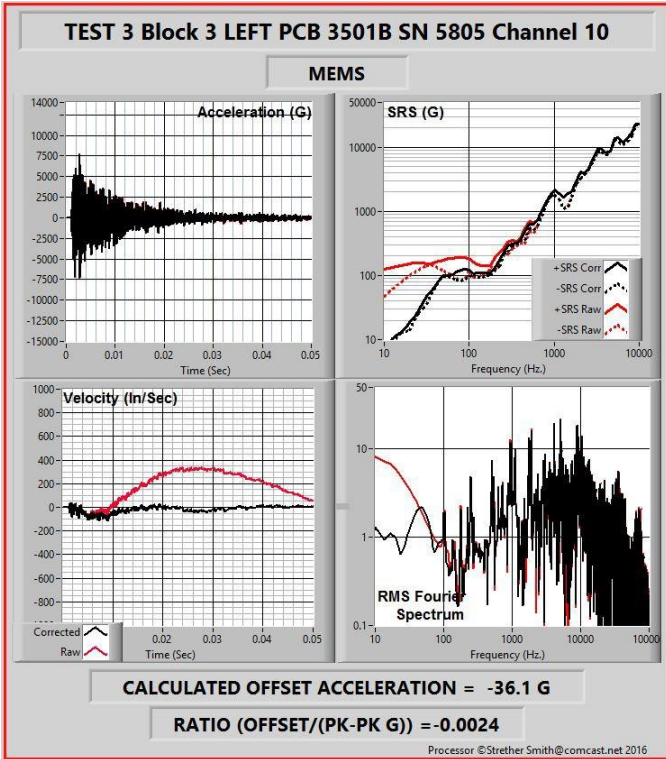


CALCULATED OFFSET ACCELERATION = 14.3 G

RATIO (OFFSET/(PK-PK G)) = 0.0011

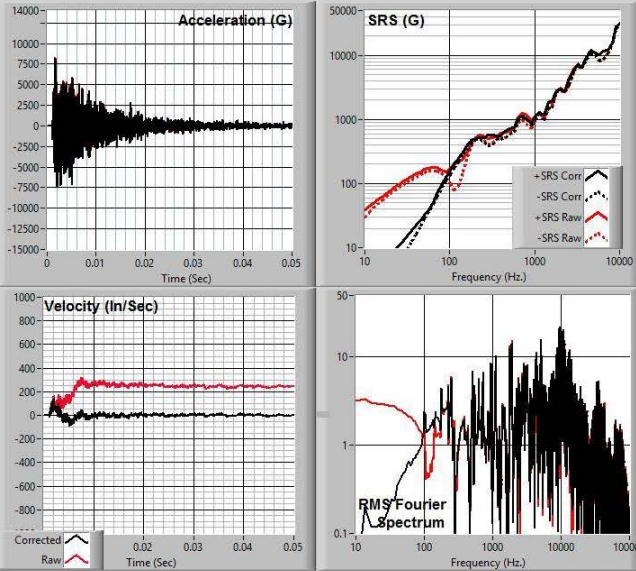
Processor ©Strether Smith@comcast.net 2016





TEST 3 Block 5 LEFT ENDEVCO 7270 SN 40423 Channel 12

MEMS



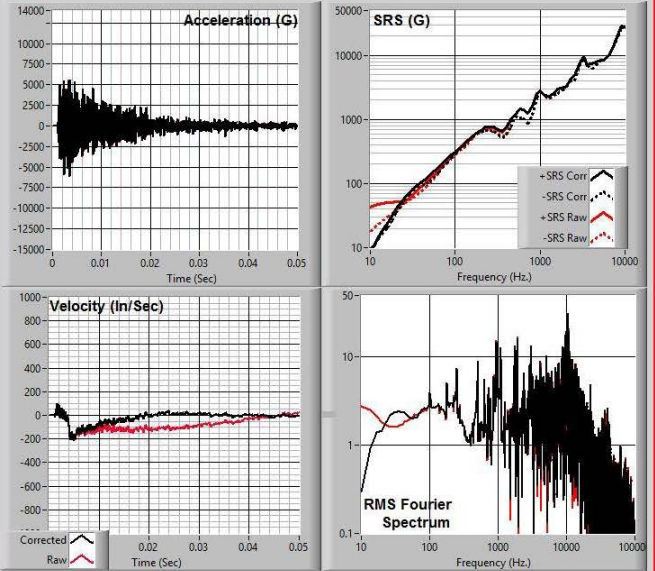
CALCULATED OFFSET ACCELERATION = -0.3 G

RATIO (OFFSET/(PK-PK G)) = -0.0000

Processor ©Strether Smith@comcast.net 2016

TEST 3 Block 5 RIGHT PCB 3991 SN 3823 Channel 14

MEMS



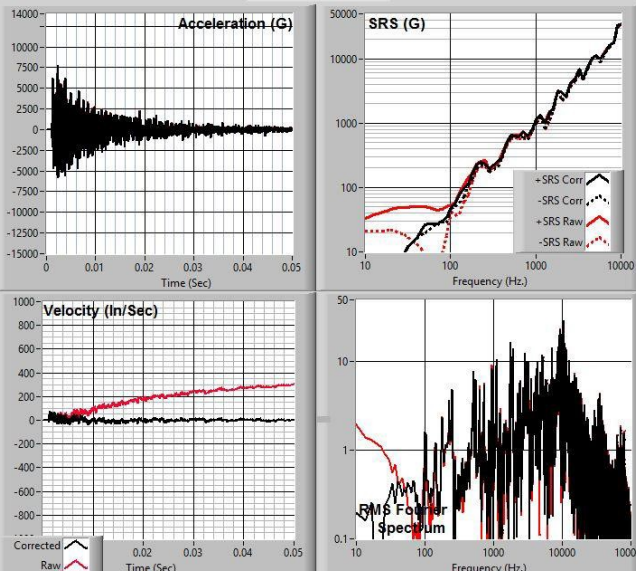
CALCULATED OFFSET ACCELERATION = 14.4 G

RATIO (OFFSET/(PK-PK G)) = 0.0012

Processor ©Strether Smith@comcast.net 2016

TEST 3 Block 6 LEFT ENDEVCO 7280 SN 41800 Channel 13

MEMS



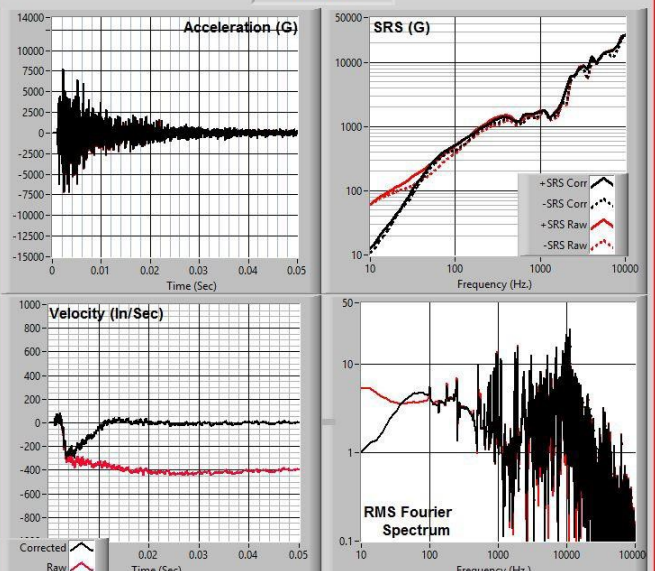
CALCULATED OFFSET ACCELERATION = 8.0 G

RATIO (OFFSET/(PK-PK G)) = 0.0006

Processor ©Strether Smith@comcast.net 2016

TEST 3 Block 6 RIGHT PCB 3991 SN 3824 Channel 15

MEMS



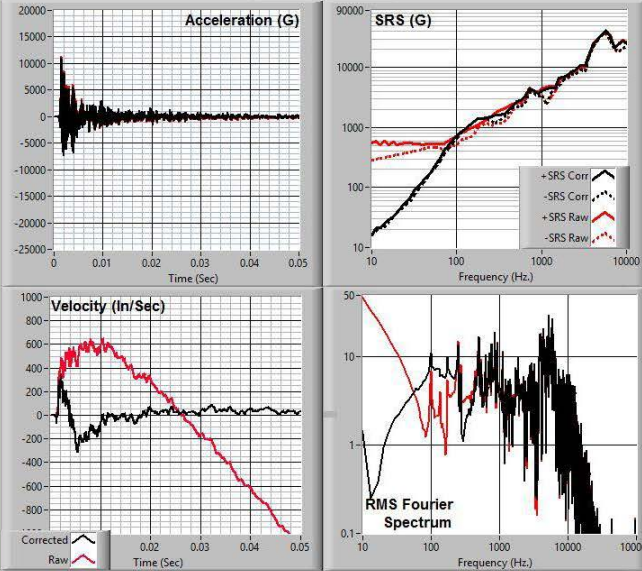
CALCULATED OFFSET ACCELERATION = 4.0 G

RATIO (OFFSET/(PK-PK G)) = 0.0003

Processor ©Strether Smith@comcast.net 2016

TEST 4 Block 1 LEFT ENDEVCO 7255 SN CF75 Channel 1

ISOL PE



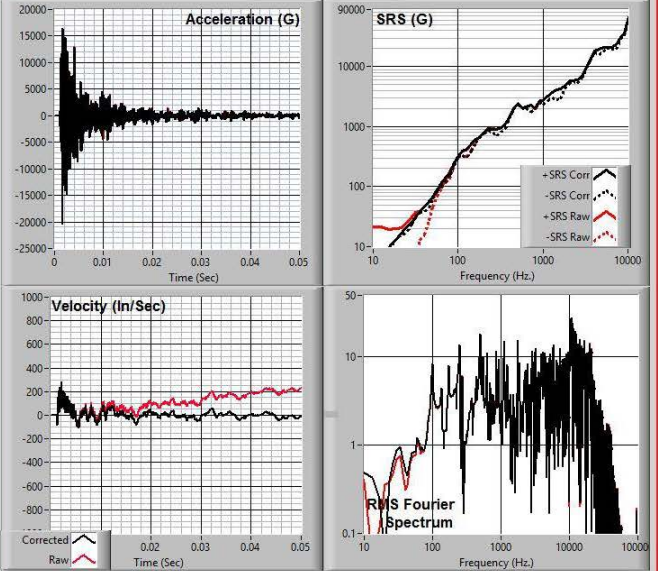
CALCULATED OFFSET ACCELERATION = -127.8 G

RATIO (OFFSET/(PK-PK G)) = -0.0070

Processor ©Strether Smith@comcast.net 2016

TEST 4 Block 1 RIGHT PCB 350B01 SN 52322 Channel 3

ISOL PE



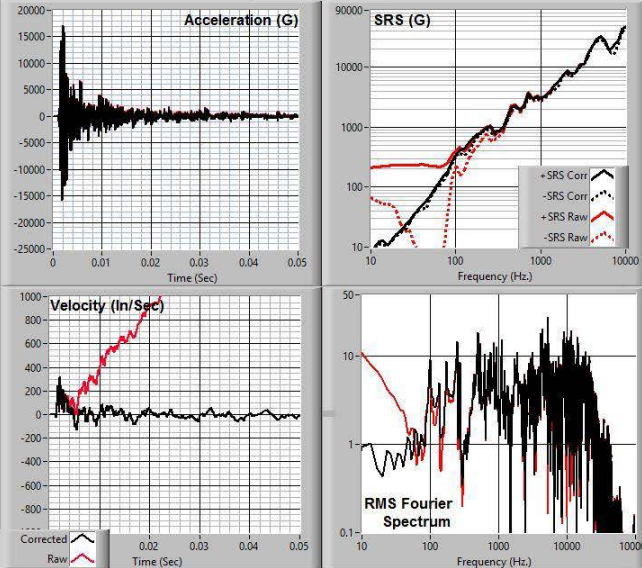
CALCULATED OFFSET ACCELERATION = 9.4 G

RATIO (OFFSET/(PK-PK G)) = 0.0003

Processor ©Strether Smith@comcast.net 2016

TEST 4 Block 2 LEFT PCB 350D02 SN 50292 Channel 6

ISOL PE



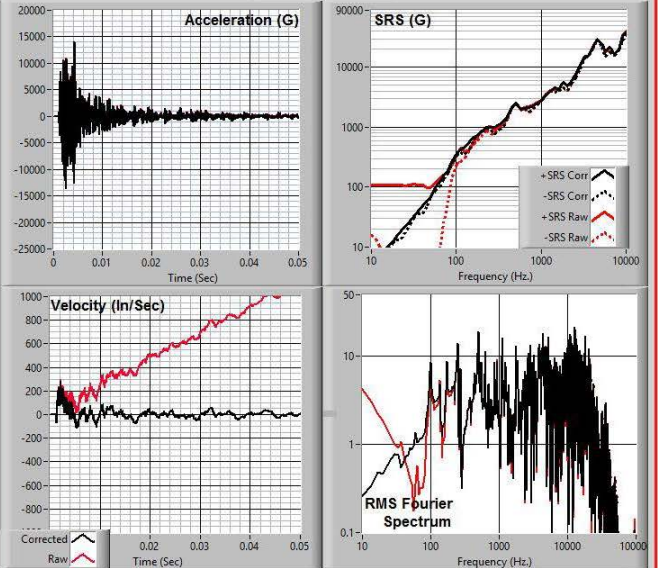
CALCULATED OFFSET ACCELERATION = 94.8 G

RATIO (OFFSET/(PK-PK G)) = 0.0029

Processor ©Strether Smith@comcast.net 2016

TEST 4 Block 2 RIGHT PCB 350B01 SN 52323 Channel 4

ISOL PE



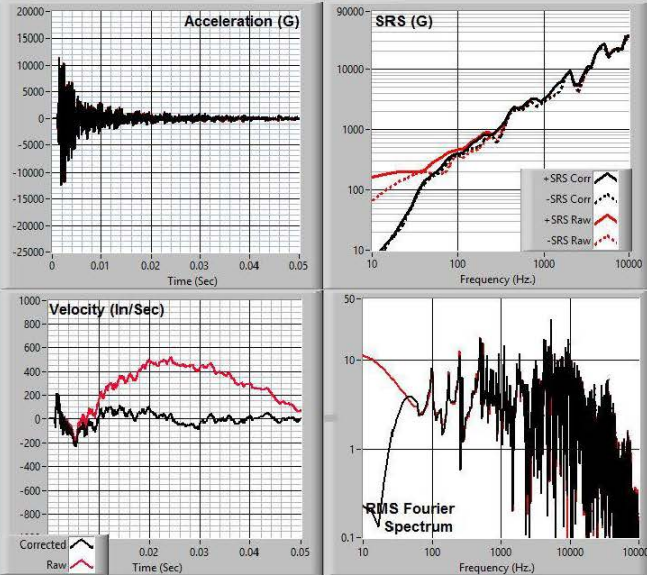
CALCULATED OFFSET ACCELERATION = 51.1 G

RATIO (OFFSET/(PK-PK G)) = 0.0018

Processor ©Strether Smith@comcast.net 2016

TEST 4 Block 3 LEFT PCB 3501B SN 5805 Channel 10

MEMS



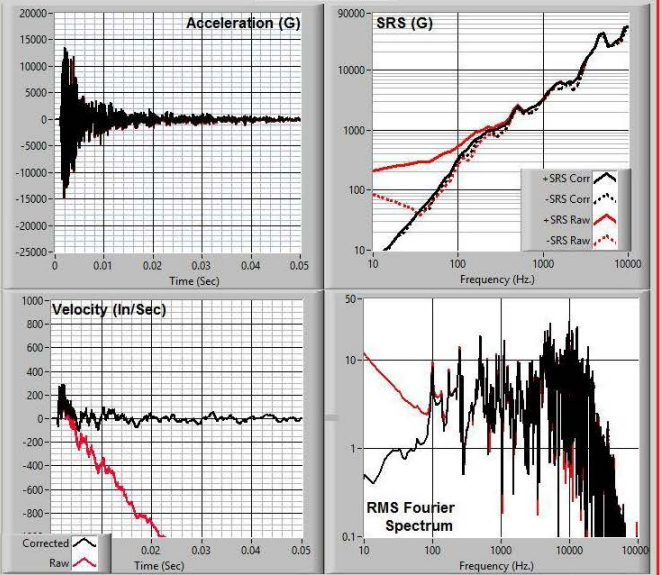
CALCULATED OFFSET ACCELERATION = -51.5 G

RATIO (OFFSET/(PK-PK G)) = -0.0022

Processor ©Strether Smith@comcast.net 2016

TEST 4 Block 3 RIGHT PCB 350D02 SN 50293 Channel 7

ISOL PE



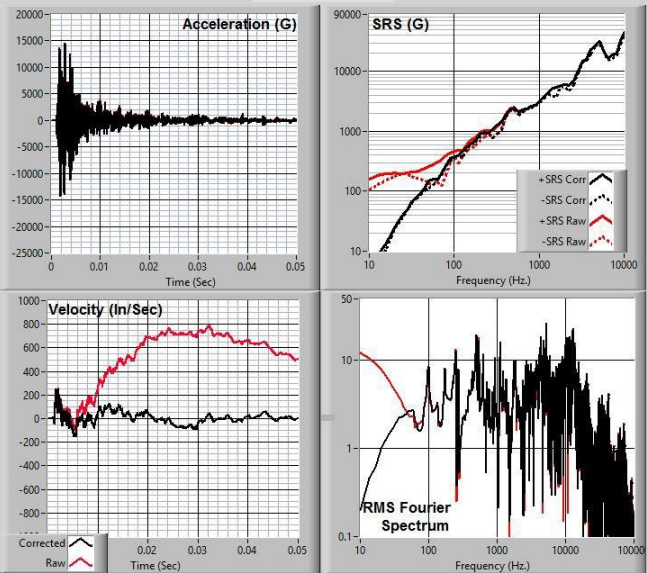
CALCULATED OFFSET ACCELERATION = -91.7 G

RATIO (OFFSET/(PK-PK G)) = -0.0032

Processor ©Strether Smith@comcast.net 2016

TEST 4 Block 4 LEFT PCB 3501B SN 5806 Channel 16

MEMS



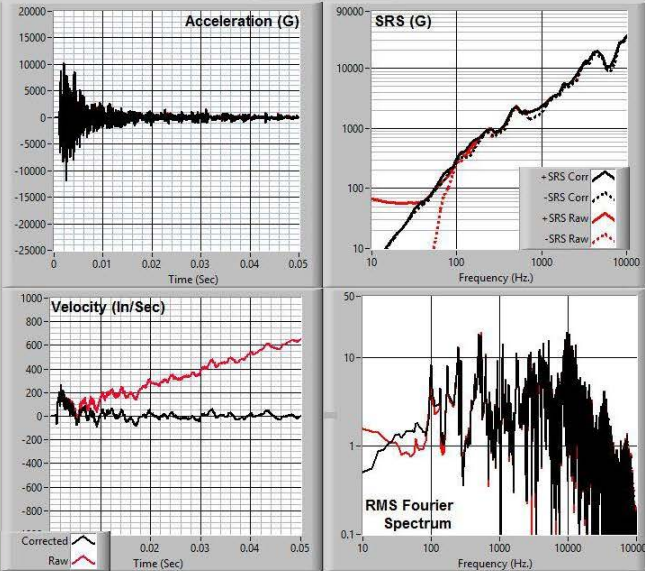
CALCULATED OFFSET ACCELERATION = -33.1 G

RATIO (OFFSET/(PK-PK G)) = -0.0011

Processor ©Strether Smith@comcast.net 2016

TEST 4 Block 5 LEFT ENDEVCO 7270 SN 40423 Channel 12

MEMS



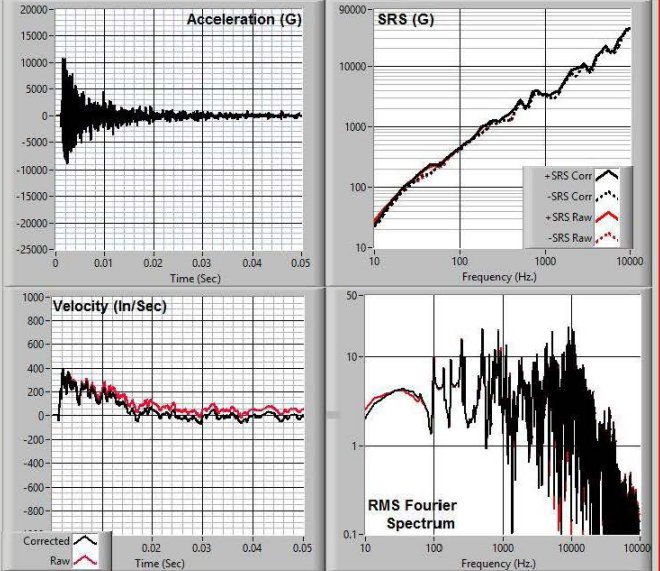
CALCULATED OFFSET ACCELERATION = 32.4 G

RATIO (OFFSET/(PK-PK G)) = 0.0015

Processor ©Strether Smith@comcast.net 2016

TEST 4 Block 5 RIGHT PCB 3991 SN 3823 Channel 14

MEMS



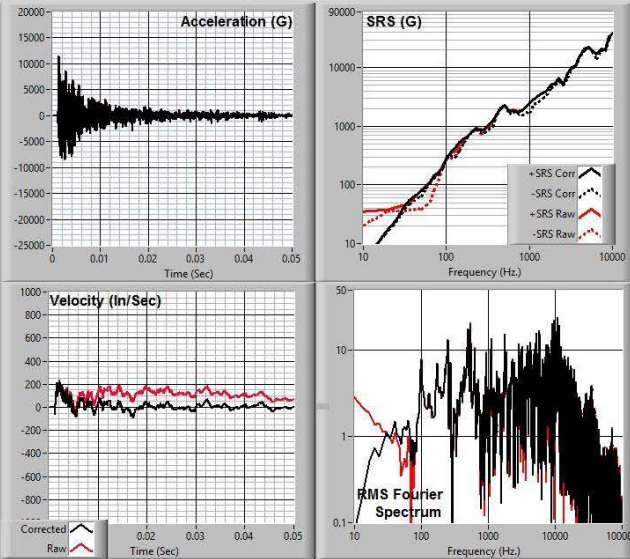
CALCULATED OFFSET ACCELERATION = -1.4 G

RATIO (OFFSET/(PK-PK G)) = -0.0001

Processor ©Strether Smith@comcast.net 2016

TEST 4 Block 6 LEFT ENDEVCO 7280 SN 41800 Channel 13

MEMS



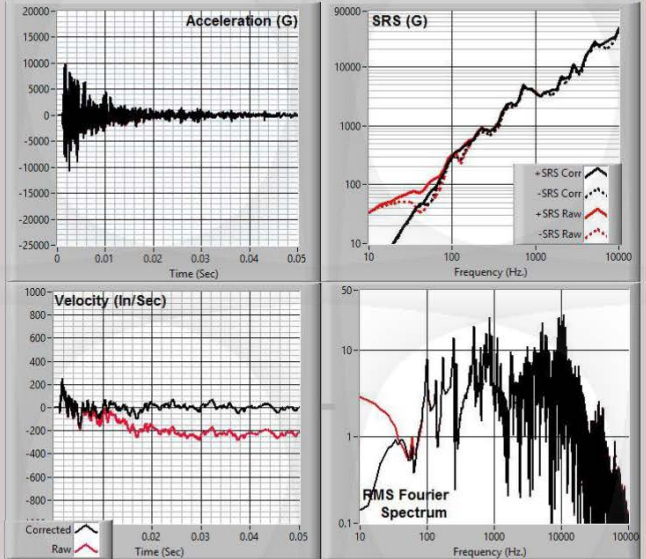
CALCULATED OFFSET ACCELERATION = -11.1 G

RATIO (OFFSET/(PK-PK G)) = -0.0006

Processor ©Strether Smith@comcast.net 2016

TEST 4 Block 6 RIGHT PCB 3991 SN 3824 Channel 15

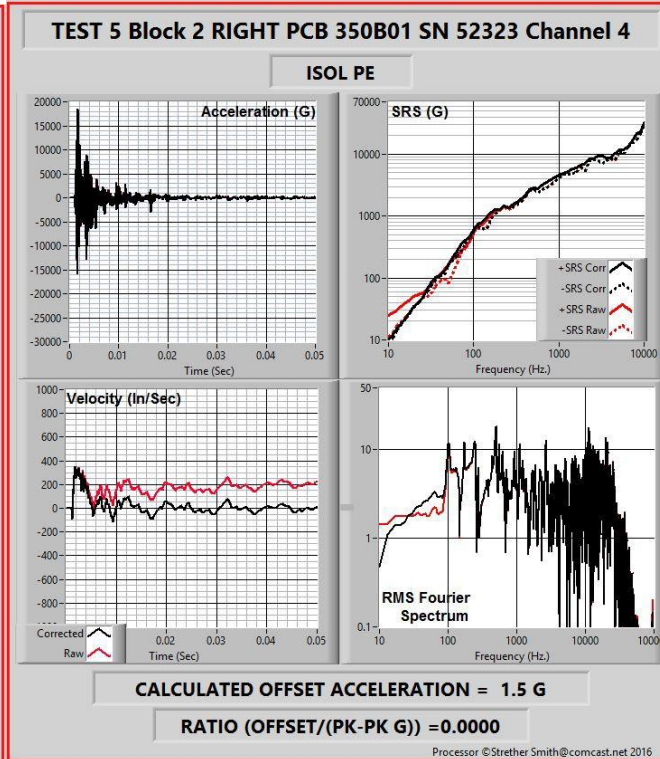
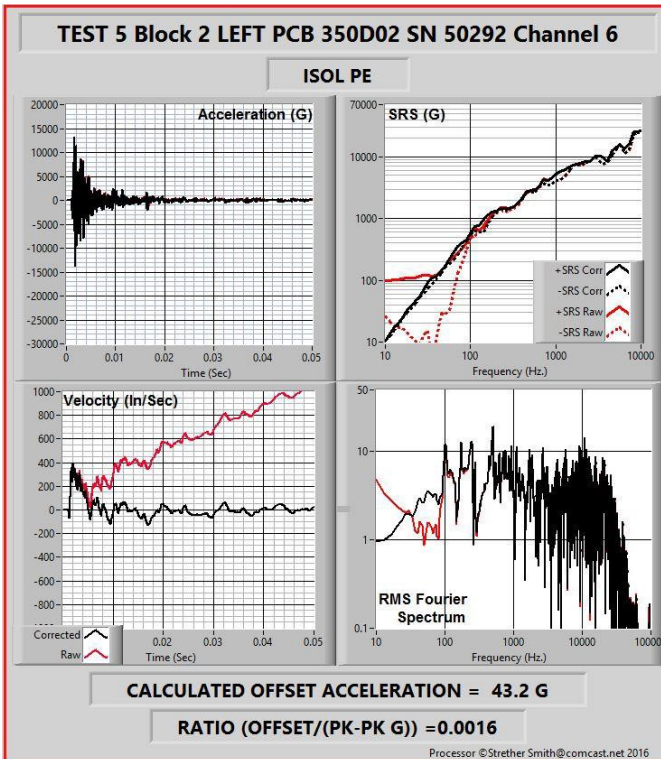
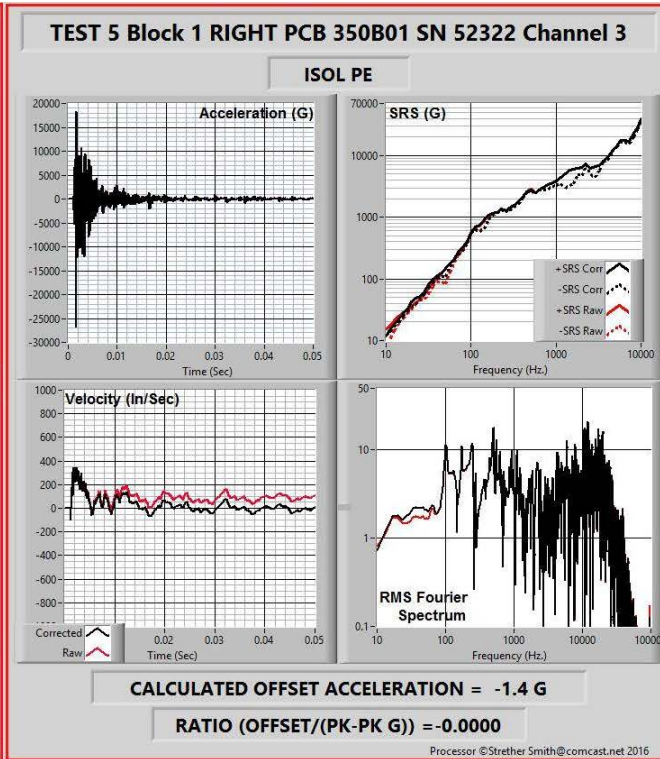
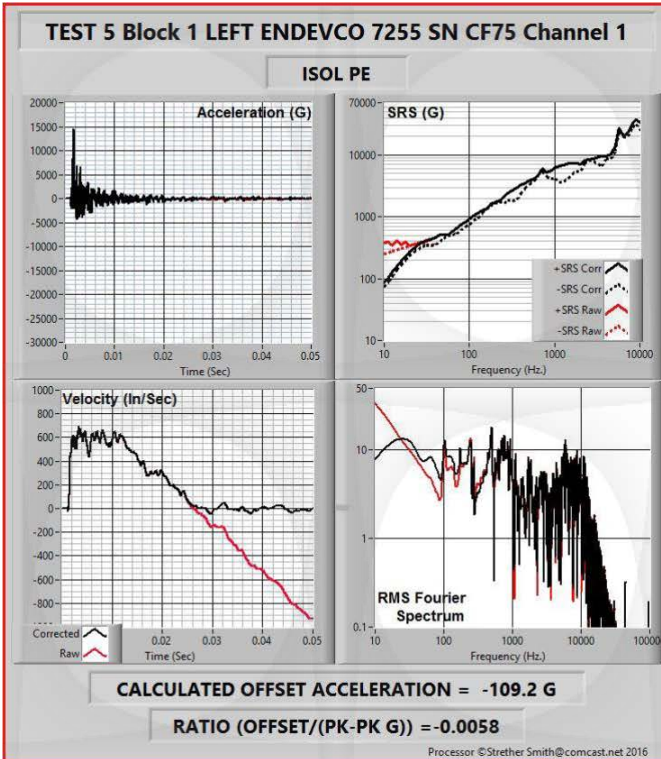
MEMS

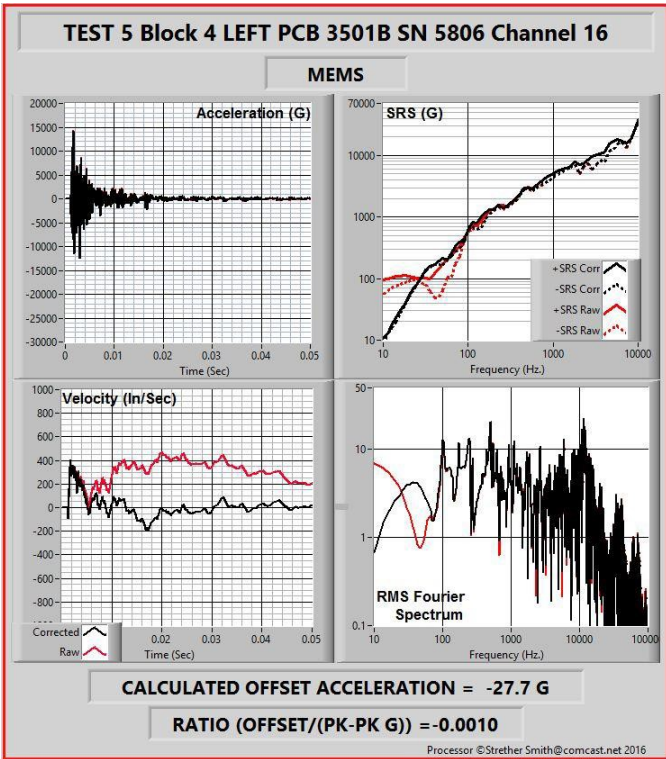
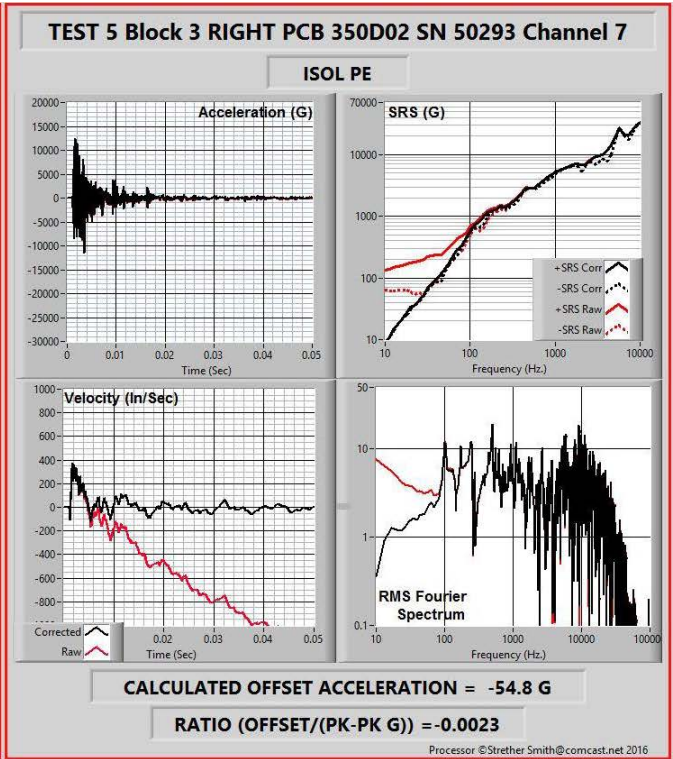
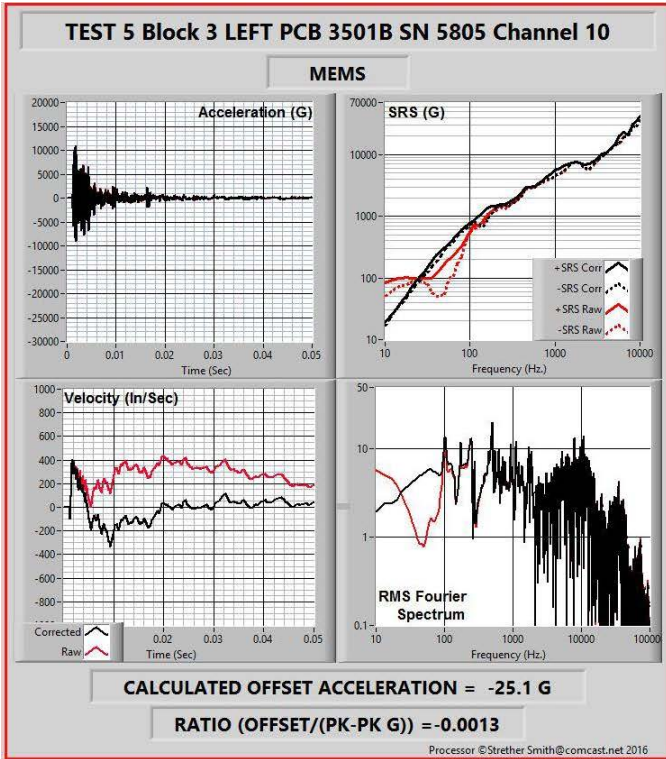


CALCULATED OFFSET ACCELERATION = -1.3 G

RATIO (OFFSET/(PK-PK G)) = -0.0001

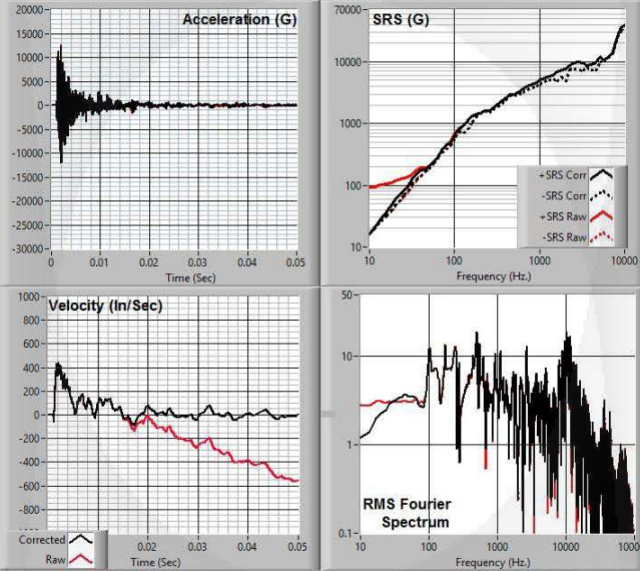
Processor ©Strether Smith@comcast.net 2016





TEST 5 Block 5 LEFT ENDEVCO 7270 SN 40423 Channel 12

MEMS



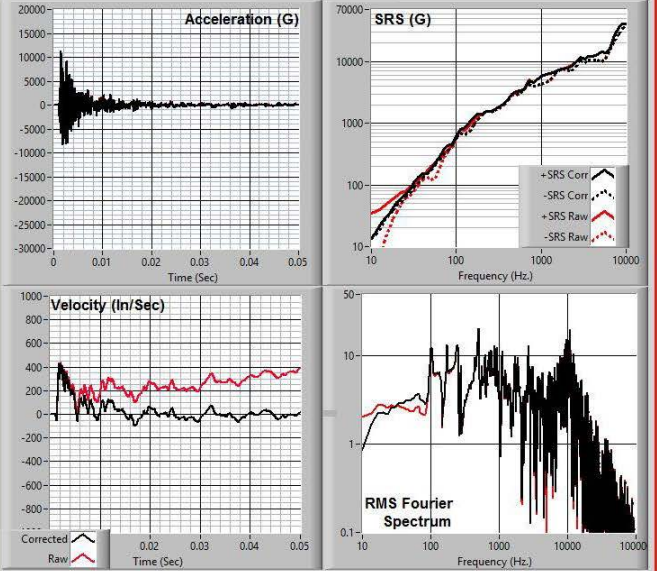
CALCULATED OFFSET ACCELERATION = -46.2 G

RATIO (OFFSET/(PK-PK G)) = -0.0019

Processor ©Strether Smith@comcast.net 2016

TEST 5 Block 5 RIGHT PCB 3991 SN 3823 Channel 14

MEMS



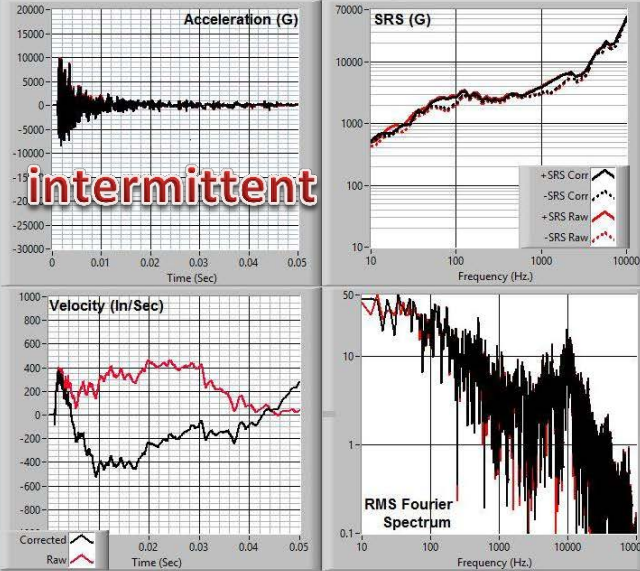
CALCULATED OFFSET ACCELERATION = 13.1 G

RATIO (OFFSET/(PK-PK G)) = 0.0007

Processor ©Strether Smith@comcast.net 2016

TEST 5 Block 6 LEFT ENDEVCO 7280 SN 41800 Channel 13

MEMS



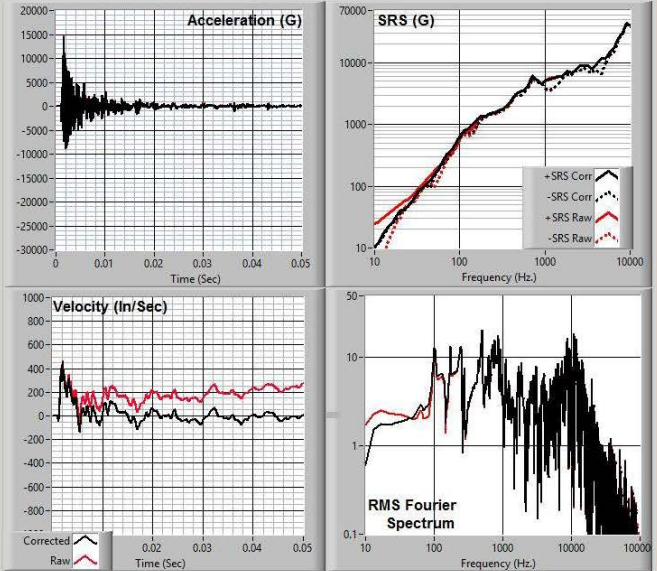
CALCULATED OFFSET ACCELERATION = -41.0 G

RATIO (OFFSET/(PK-PK G)) = -0.0022

Processor ©Strether Smith@comcast.net 2016

TEST 5 Block 6 RIGHT PCB 3991 SN 3824 Channel 15

MEMS



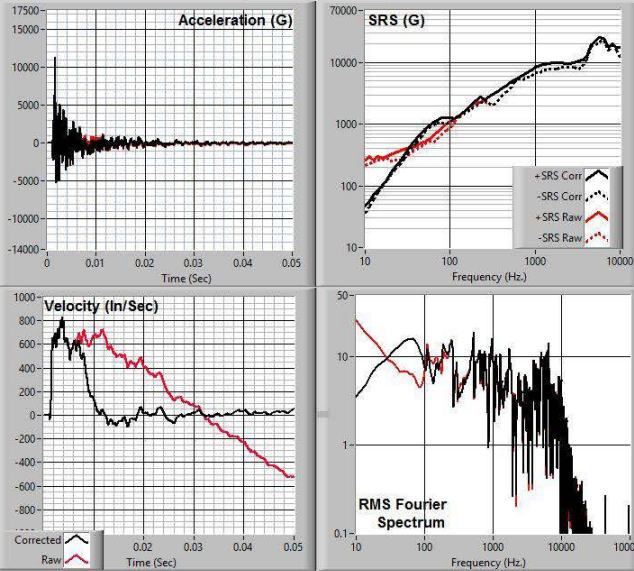
CALCULATED OFFSET ACCELERATION = 7.5 G

RATIO (OFFSET/(PK-PK G)) = 0.0003

Processor ©Strether Smith@comcast.net 2016

TEST 6 Block 1 LEFT ENDEVCO 7255 SN CF75 Channel 1

ISOL PE



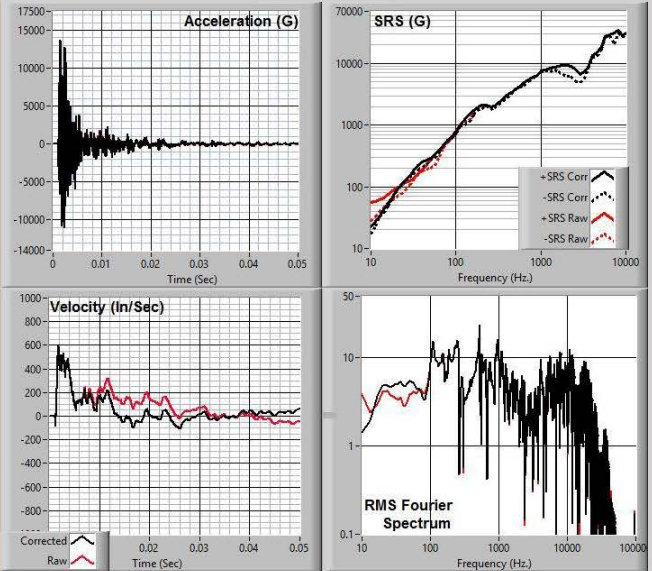
CALCULATED OFFSET ACCELERATION = -80.0 G

RATIO (OFFSET/(PK-PK G)) = -0.0048

Processor ©Strether Smith@comcast.net 2016

TEST 6 Block 1 RIGHT PCB 350B01 SN 52322 Channel 3

ISOL PE



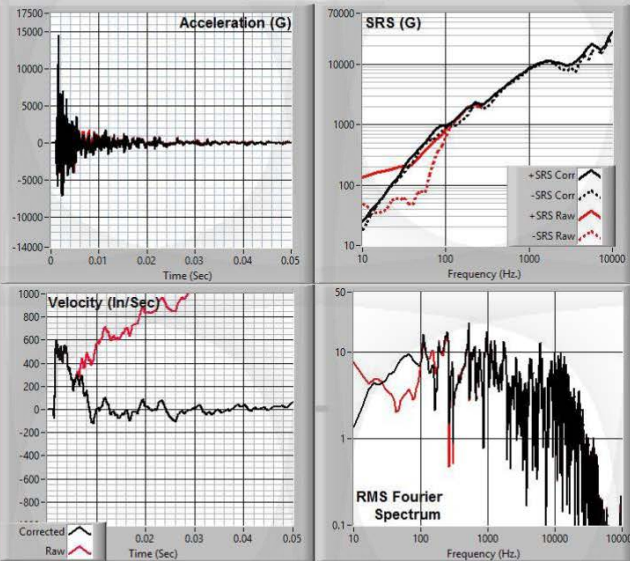
CALCULATED OFFSET ACCELERATION = -13.8 G

RATIO (OFFSET/(PK-PK G)) = -0.0006

Processor ©Strether Smith@comcast.net 2016

TEST 6 Block 2 LEFT PCB 350D02 SN 50292 Channel 6

ISOL PE



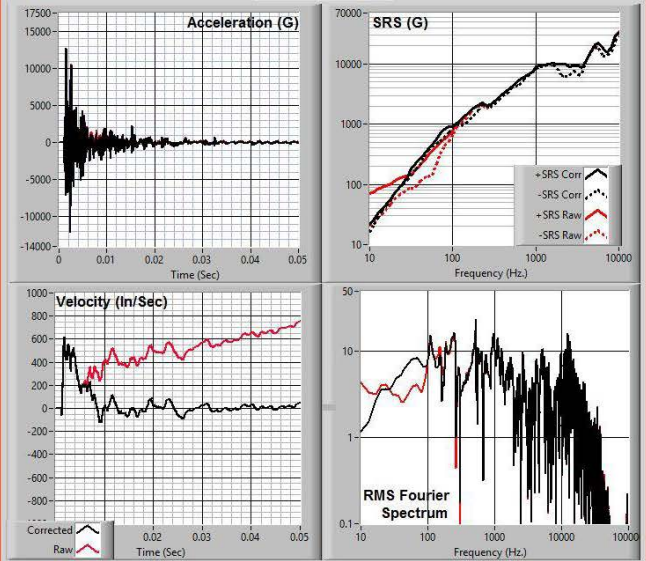
CALCULATED OFFSET ACCELERATION = 56.7 G

RATIO (OFFSET/(PK-PK G)) = 0.0026

Processor ©Strether Smith@comcast.net 2016

TEST 6 Block 2 RIGHT PCB 350B01 SN 52323 Channel 4

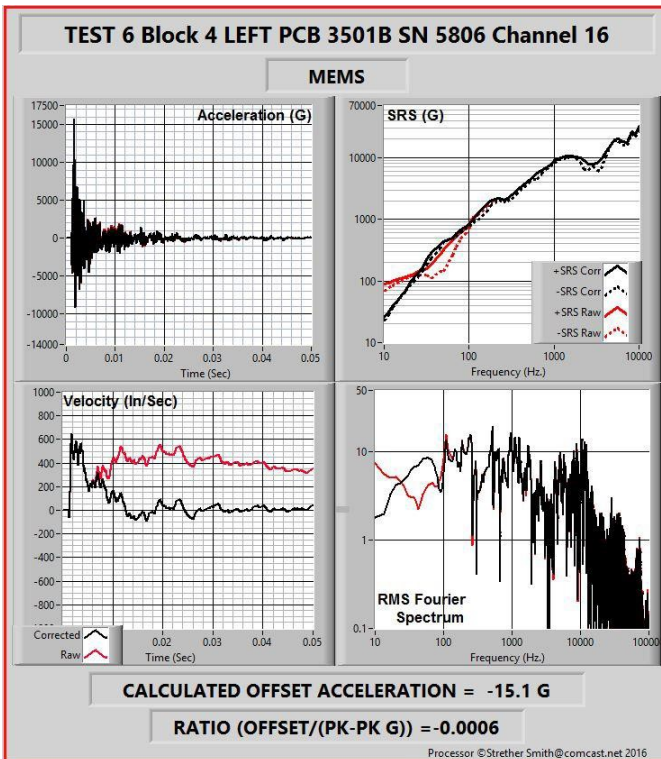
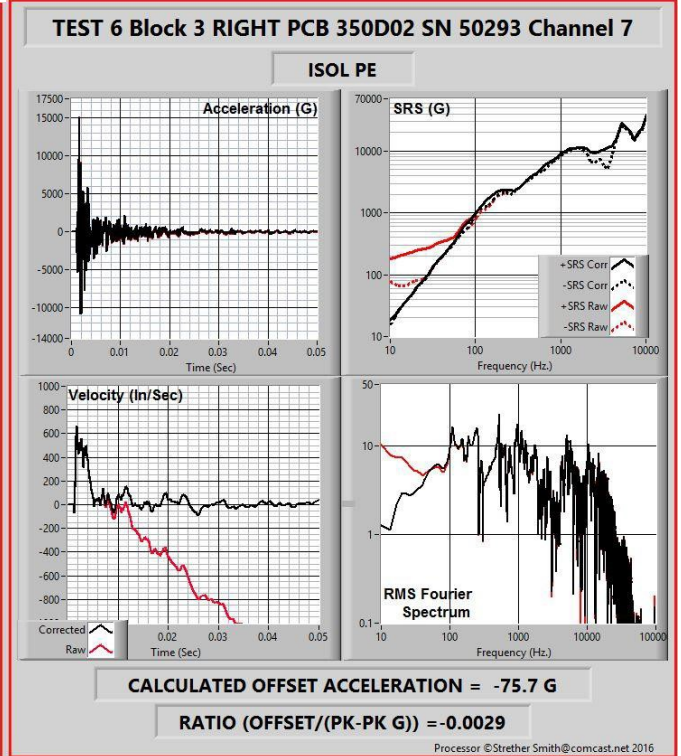
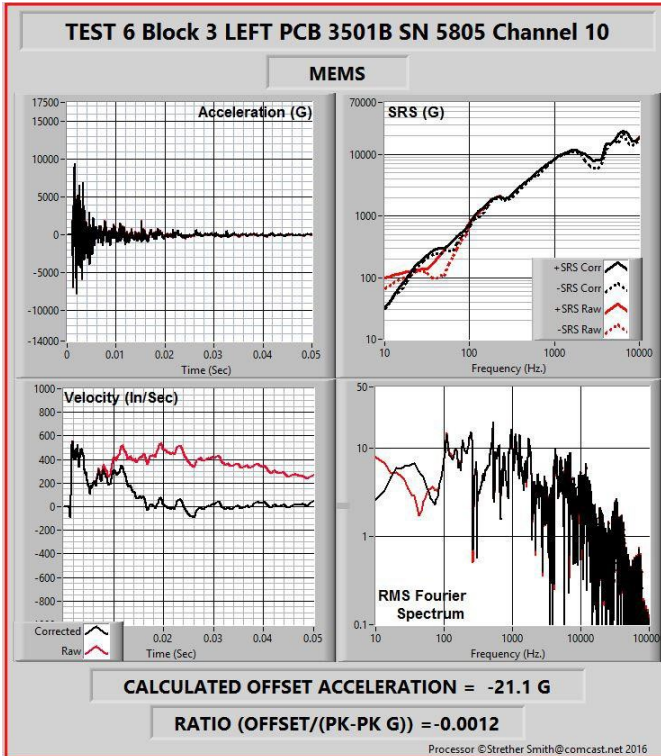
ISOL PE



CALCULATED OFFSET ACCELERATION = 24.5 G

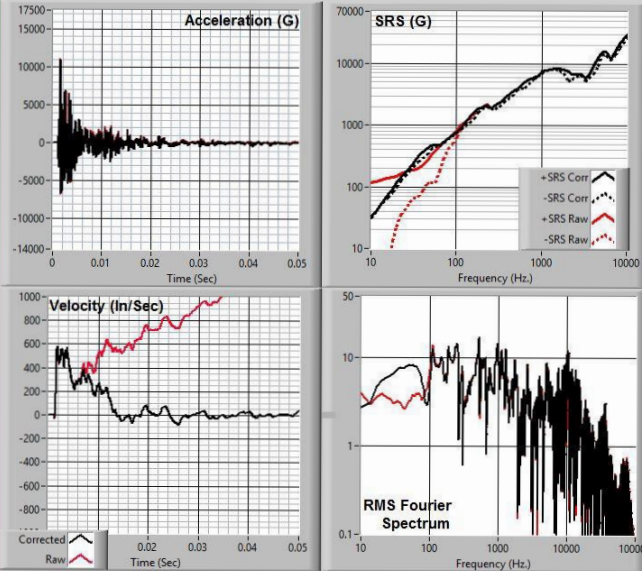
RATIO (OFFSET/(PK-PK G)) = 0.0010

Processor ©Strether Smith@comcast.net 2016



TEST 6 Block 5 LEFT ENDEVCO 7270 SN 40423 Channel 12

MEMS



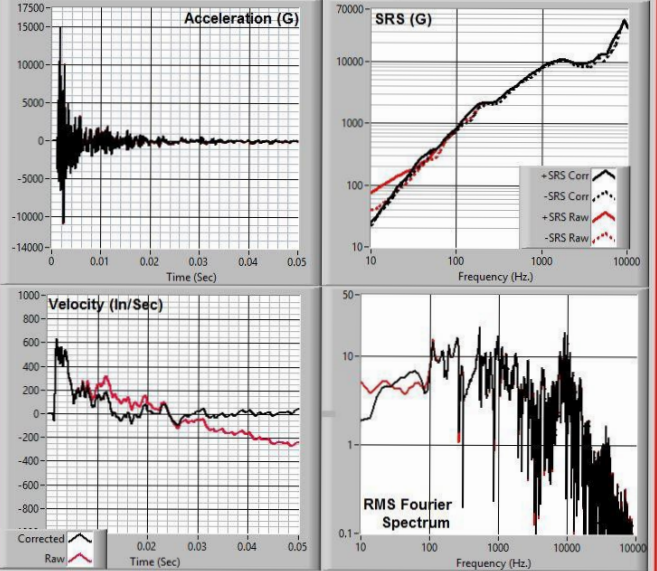
CALCULATED OFFSET ACCELERATION = 61.1 G

RATIO (OFFSET/(PK-PK G)) = 0.0034

Processor ©Strether Smith@comcast.net 2016

TEST 6 Block 5 RIGHT PCB 3991 SN 3823 Channel 14

MEMS



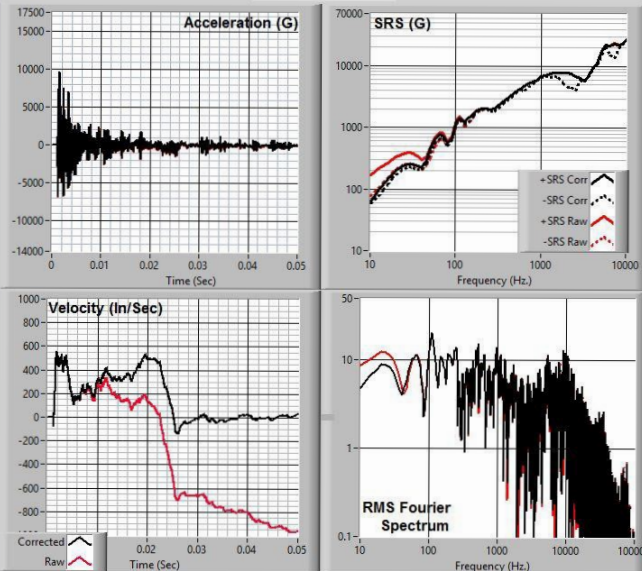
CALCULATED OFFSET ACCELERATION = -24.3 G

RATIO (OFFSET/(PK-PK G)) = -0.0009

Processor ©Strether Smith@comcast.net 2016

TEST 6 Block 6 LEFT ENDEVCO 7280 SN 41800 Channel 13

MEMS



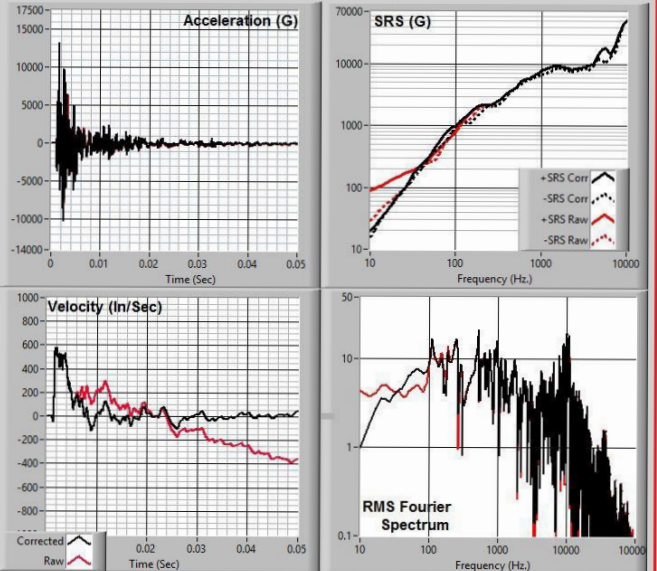
CALCULATED OFFSET ACCELERATION = -40.7 G

RATIO (OFFSET/(PK-PK G)) = -0.0025

Processor ©Strether Smith@comcast.net 2016

TEST 6 Block 6 RIGHT PCB 3991 SN 3824 Channel 15

MEMS



CALCULATED OFFSET ACCELERATION = -33.0 G

RATIO (OFFSET/(PK-PK G)) = -0.0014

Processor ©Strether Smith@comcast.net 2016



3425 Walden Avenue, Depew, NY 14043 USA

pcb.com | info@pcb.com | 800 828 8840 | +1 716 684 0001

© 2024 PCB Piezotronics - all rights reserved. PCB Piezotronics is a wholly-owned subsidiary of Amphenol Corporation. Endevo is an assumed name of PCB Piezotronics of North Carolina, Inc., which is a wholly-owned subsidiary of PCB Piezotronics, Inc. Accumetrics, Inc. and The Modal Shop, Inc. are wholly-owned subsidiaries of PCB Piezotronics, Inc. IMI Sensors and Larson Davis are Divisions of PCB Piezotronics, Inc. Except for any third party marks for which attribution is provided herein, the company names and product names used in this document may be the registered trademarks or unregistered trademarks of PCB Piezotronics, Inc., PCB Piezotronics of North Carolina, Inc. (d/b/a Endevo), The Modal Shop, Inc. or Accumetrics, Inc. Detailed trademark ownership information is available at www.pcb.com/trademarkownership.

WPL_60_0324